Helsinki University of Technology
Materials Physics Laboratory
Espoo 2003

PROPAGATION-INVARIANT WAVES IN ACOUSTIC, OPTICAL, AND RADIO-WAVE FIELDS

Janne Salo

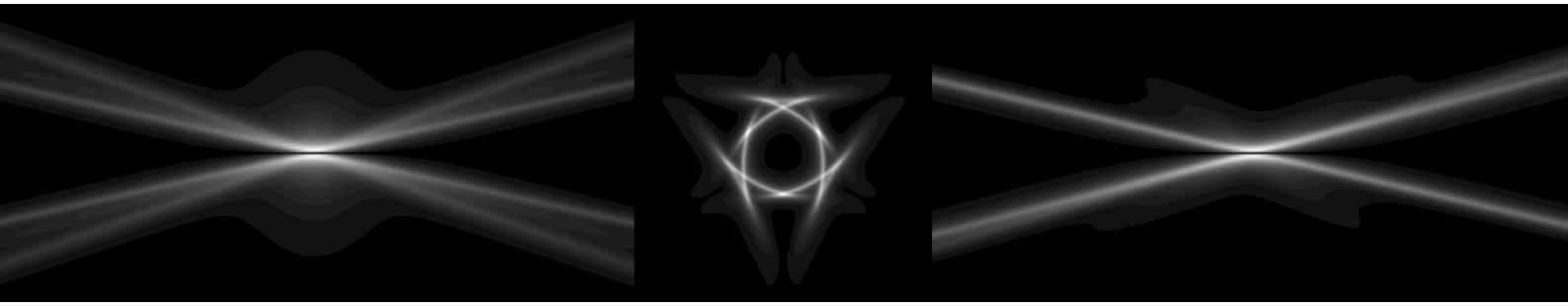

TEKNILLINEN KORKEAKOULU
TEKNISKA HÖGSKOLAN
HELSINKI UNIVERSITY OF TECHNOLOGY
TECHNISCHE UNIVERSITÄT HELSINKI
UNIVERSITE DE TECHNOLOGIE D'HELSINKI

Helsinki University of Technology Publications in Engineering Physics

Teknillisen korkeakoulun teknillisen fysiikan julkaisuja

Espoo 2003 TKK-F-A819

PROPAGATION-INVARIANT WAVES IN ACOUSTIC, OPTICAL, AND RADIO-WAVE FIELDS

Janne Salo

Dissertation for the degree of Doctor of Technology to be presented with due permission for public examination and debate in Auditorium F1 at Helsinki University of Technology (Espoo, Finland) on the 18th of January, 2003, at 12 o'clock noon.

Helsinki University of Technology
Department of Engineering Physics and Mathematics
Materials Physics Laboratory

Teknillinen korkeakoulu
Teknillisen fysiikan ja matematiikan osasto
Materiaalifysiikan laboratorio

Distribution:
Helsinki University of Technology
Materials Physics Laboratory
P.O. Box 2200
FIN-02015 HUT
Tel. +358-9-451-5650
Fax. +358-9-451-3164
E-mail: Janne.Salo@hut.fi

ISBN 951-22-6292-4 (printed)
ISBN 951-22-6293-2 (pdf)
ISSN 1456-3320

Otamedia Oy
Espoo 2003

HELSINKI UNIVERSITY OF TECHNOLOGY P.O. BOX 1000, FIN-02015 HUT http://www.hut.fi	ABSTRACT OF DOCTORAL DISSERTATION

Author Janne Oskari Salo

Name of the dissertation
Propagation-invariant waves in acoustic, optical, and radio-wave fields

Date of manuscript 15.10.2002	Date of the dissertation 18.1.2003
☐ Monograph	☑ Article dissertation (summary + original articles)

Department	Engineering Physics and Mathematics
Laboratory	Materials Physics Laboratory
Field of research	Diffraction-free wave propagation
Opponent(s)	Prof. Rafael Piestun
Supervisor	Prof. Martti M. Salomaa
(Instructor)	

Abstract

The physical phenomena considered in this thesis are associated with electromagnetic and acoustic waves that propagate in free space or in homogeneous media without diffraction. The concept of rotationally periodic wave propagation is introduced in the first journal article included in the thesis and it is subsequently used to analyse waves that avoid diffractive deterioration by repeatedly returning to their initial shape, possibly rotated around the optical axis. Such waves constitute an essential generalisation to several kinds of acoustic and optical beams, such as Bessel beams and self-imaging waves. Additionally, rotationally periodic waves also comprise pulsed wave forms that may propagate with a velocity independent of the speed of light (or sound) in the particular medium. This does not, however, lead to any violation of relativistic principles, as the pulse is continuously reformed by signals that have synchronously been transmitted from different locations. The individual articles in this dissertation mainly concentrate on the properties of pulsed waves.

Two specific issues are also treated in the dissertation: (i) Acoustic nondiffracting waves are considered in anisotropic, piezoelectric crystals. Their propagation may differ drastically from that of ordinary (plane) waves, and nondiffracting waves may also include effects such as internal diffraction, phonon focusing, and caustics. Possible transducer structures are considered for the generation of nondiffracting waves into bulk crystals. (ii) Generation of Bessel beams have also been verified with the use of radio holograms in the millimetre-wave regime. Hologram techniques developed have allowed the investigation of various other wave forms and their propagation, such as tapered plane waves and radio-wave vortices. A back-propagation algorithm has also been introduced for designing holograms that form wave fields of an arbitrary design.

Keywords	Nondiffracting waves, Bessel beams, X waves, bulk-acoustic waves, radio holograms		
UDC	534.2, 537.87	Number of pages	58
ISBN (printed)	951-22-6292-4	ISBN (pdf)	951-22-6293-2
ISBN (others)		ISSN	1456-3320
Publisher	Helsinki University of Technology, Materials Physics Laboratory		
Print distribution			
☑ The dissertation can be read at http://lib.hut.fi/Diss/			

Preface

All the research for this dissertation has been carried out in the Materials Physics Laboratory at the Helsinki University of Technology, except for a brief visit to the Royal Institute of Technology in Stockholm, Sweden. The work has financially been supported by the Research Council of the Helsinki University of Technology, the Finnish Cultural Foundation, the Jenny and Antti Wihuri Foundation, the Swedish-Finnish Cultural Foundation, and the Foundation of Technology (Finland). I would also like to thank the Graduate School in Technical Physics for accommodating my graduate studies and research, and the Magnus Ehrnrooth Foundation for an opportunity to carry on with scientific work after the completion of the dissertation.

Professor Martti M. Salomaa has been my steadfast supervisor and instructor from the very beginning of my work at the University and I am greatly indebted to him for his support and help through the preparation and writing of this dissertation (and earlier theses), as well as for all his efforts on the excellent working environment in general. I also express my gratitude to professor Ari T. Friberg for uncompromising discussions on my work, to Dr. Tech. Juha Fagerholm for his guidance during the Master's Thesis and at the early stage of the subsequent research, and to professor Antti V. Räisänen for his contribution to the experimental work.

I am also grateful for all the other coauthors, both from the Materials Physics Laboratory and from the Radio Laboratory, for fruitful collaboration. I am equally grateful for all the other present and former members of the Laboratory, as well as for other coworkers, for scientific discussions, and much beyond, that, I hope, they have enjoyed as much as I have.

Finally, I thank my friends for everything we have done together, and my family, especially my mother, for letting me grow to what I am.

Espoo, January 2003

Janne Salo

List of publications

This dissertation is a review of the author's work in the fields of nondiffracting waves and radio-hologram technology. It consists of an overview and the following selection of publications in these fields:

I J. Salo and M. M. Salomaa: "Diffraction-free pulses at arbitrary speeds", *Journal of Optics A*, September 2001, vol. **3**, no. 5, pp. 366-373.

II J. Salo and M. M. Salomaa: "Subsonic nondiffracting waves", *Acoustics Research Letters Online*, January 2001, vol. **2**, issue 1, pp. 31-36.

III J. Salo, J. Fagerholm, A. T. Friberg, and M. M. Salomaa: "Unified Description of Nondiffracting X and Y Waves", *Physical Review E*, September 2000, vol. **62**, no. 3, pp. 4261-4275.

IV J. Salo, A. T. Friberg, and M. M. Salomaa: "Orthogonal X waves", *Journal of Physics A*, November 2001, vol. **34**, no. 43, pp. 9319-9327.

V J. Salo, J. Fagerholm, A. T. Friberg, and M. M. Salomaa: "Nondiffracting Bulk-Acoustic X waves in Crystals", *Physical Review Letters*, August 1999, vol. **83**, no. 6, pp. 1171-1174.

VI J. Salo and M. M. Salomaa: "Nondiffracting Waves in Anisotropic Media", Report TKK-F-A817, 2002, submitted for publication.

VII J. Salo, J. Meltaus, E. Noponen, J. Westerholm, M. M. Salomaa, A. Lönnqvist, J. Säily, J. Häkli, J. Ala-Laurinaho, and A. V. Räisänen: "Millimetre-wave Bessel beams using computer holograms", *Electronics Letters*, June 2001, vol. **37**, issue 13, pp. 834-835.

VIII J. Salo, J. Meltaus, E. Noponen, M. M. Salomaa, A. Lönnqvist, T. Koskinen, V. Viikari, J. Säily, J. Häkli, J. Ala-Laurinaho, J. Mallat and A. V. Räisänen: "Holograms for shaping radio-wave fields", *Journal of Optics A*, September 2002, vol. **4**, no. 5, pp. S161-S167.

Throughout the overview, these publications are referred to by their Roman numerals.

Author's contributions

I have written essential parts of the papers [I]–[VII] and acted as an editor for the paper [VIII] that was written sectionwise by several authors.

As a subject of my master's thesis, I was given the problem of the possible existence of nondiffracting waves in anisotropic crystals. I found the answer to be positive and the formulation of the theory was published in [V] (chronologically the first paper of the thesis); for this I am greatly indebted to my coauthors as seniour physicists without whom the result would never have been put in the proper context within the field of physics.

My second paper, [III], was based on the coauthors' preliminary result that many previously-known X waves were describable in terms of generalised hypergeometric functions. The subject began to expand, yielding a 'unified description of nondiffracting waves' that included various details of temporal and spatial properties of the X waves.

Four subsequent theoretical papers, [II], [I], [IV], and [VI], in the chronological order, were grounded by the first two articles and their contents are entirely based on my original work.

The first experiment on Bessel beams using radio holograms, published in [VII], was schematically designed by myself, the hologram synthesis algorithm was independently implemented by myself and E. N., and the hologram was measured by members of the Radio laboratory group.

The last of the eight papers, [VIII], is, essentially, a summary of results obtained using hologram techniques in millimetre-wave regime. In addition to being the editor of the article, I have been strongly involved in the design of all new experiments published in this paper, as well as in the analysis of the measurement results obtained.

Foreword

This thesis consists of an introduction and eight first-author articles. They treat four different aspects of localised wave propagation: (i) a general theory of localised, periodic pulse propagation in free space (including the special case of subluminal wave modes), (ii) superluminal X waves that are localised and invariant under propagation, (iii) mathematical existence of anisotropic nondiffracting waves, together with their possible methods of generation in piezoelectric crystals, and (iv) use of radio holograms in the generation of nondiffracting and other beams in the millimetre-wave regime.

At this point I need to comment on the terminology used. Durnin originally introduced the terms 'nondiffracting wave' and 'diffraction-free' beam motivated by the fact the *central* maximum of the beam appeared to propagate without diffractive spreading. These names are, however, sometimes considered unfortunate for two reasons: First of all, any finite-aperture (or finite-energy) realisation of these beams is, eventually, bound to diffract. Hence, the term 'propagation-invariant' is also misleading, as well as the term 'limited-diffraction' that suggests that these waves are only subject to minor diffraction effects. Secondly, they are by no means nondiffracting in the sense that they would not diffract upon incidence on any sort of grating or other obstacle. Also their localisation is questionable: however extensive a volume (or large an area) is considered around the centre of an even mathematically ideal beam or pulse, it yet contains a vanishing portion of the entire wave energy. This having been said, I wish to use the more or less standard terminology on the subject and to take the freedom of using terms such as 'nondiffracting', 'diffraction-free', 'localised', 'propagation-invariant' etc. where I find them convenient.

Contents

Preface **v**

List of publications **vi**

Author's contribution **vii**

Foreword **viii**

Contents **ix**

1 Introduction **1**
1.1 Brief history of localised waves 1

2 Periodically propagating waves **5**
2.1 Bessel beams 5
2.2 Periodic wave modes 7
2.3 Nondiffracting X waves 11
2.4 Focus-wave modes 13
2.5 Other localised wave modes 14

3 Acoustic waves in anisotropic crystals **17**
3.1 Anisotropic wave propagation 17
3.2 Nondiffracting waves 21
3.2.1 Generation of anisotropic NDWs 24

4 Radio-hologram techniques **27**
4.1 Diffractive elements 27
4.1.1 Choosing the desired transmittance 28
4.1.2 Quantisation of the hologram structure 31
4.2 Experimental results 33
4.2.1 Plane-wave vortex 33
4.2.2 Bessel beam 34
4.2.3 Custom-made wave field 36

5 Summary **37**

Bibliography **39**

Abstracts of publications I–VIII **47**

1 Introduction

Diffraction is an ever-present phenomenon that affects the propagation of waves in two- or higher-dimensional homogeneous media: all deviations from transverse uniformity will, eventually, corrupt the wave profile, leading to the separation of wave components that move into different directions[1]. The best-known examples are the widening of a Gaussian beam and the sinc-pattern formed by a sharply bounded square aperture.

The strength of such a deterioration is proportional to the length scale of spatial variations of the wave field, compared with the wavelength. Pulse-like waves, formed as wave packets comprising a continuum of wavelengths, are equally subject to diffraction. The only wave-form totally devoid of diffractive effects was thought to be the one with no transverse variations, i.e., a plane wave. Hence it came as a very surprise when Durnin & *al.* in 1987 published an experimental measurement of a diffraction-free light beam [1]. Its name owed to the fact that the central peak on the optical axis appeared to defy the effect of diffraction despite its spot size on the order of a wavelength.

The properties of such a peculiar light beam were promptly searched for. It was readily noted that a truly diffraction-free beam would require an infinite aperture. Even though the beam intensity is peaked on the optical axis, there should be an infinite number of side lobes (of decreasing brightness) to support the main beam. Limiting their number unavoidably also limits the length of the 'diffraction-free' beam, making it, again, subject to diffraction.

Figure 1.1 illustrates the difference between an ordinary Gaussian beam and an apertured diffraction-free beam. Although a Gaussian beam can easily be focused into a bright focal spot, it will rapidly dissolve after the focus. A diffraction-free beam, on the other hand, supports a long focal line, together with additional side lobes. The total energy carried by the latter beam is, however, much higher if equal intensity is to be achieved along the axis.

1.1 Brief history of localised waves

After Durnin's experimental demonstration of what appeared to be a nondiffracting beam, several physicists have been engaged in studying the properties and potential applications of this discovery. Nevertheless, the very same wave solution had already been published by Stratton in 1941 as a 'wave function of the circular cylinder' [3] the radial form of which was described by Bessel functions[2,3]. Hence the special functions

[1] Diffraction does not occur in one spatial dimension since no such separation is possible.

[2] Or other circular cylinder functions, depending on the radial boundary conditions.

[3] The same wave solution was also reckoned by van Nie in 1964 [4].

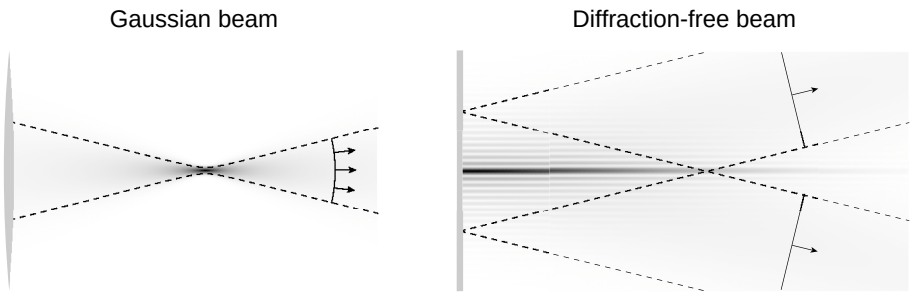

Figure 1.1: Gaussian beam and finite diffraction-free beam (represented here with a Bessel-Gauss beam [2]). The central maximum of the latter beam has the same width as the waist of the Gaussian beam. The gray-scale shading denotes the absolute value of the wave amplitude and the arrows denote the direction of energy propagation.

originally discovered by Friedrich Wilhelm Bessel in the early nineteenth century in the context of indirectly perturbed planetary motion were found to describe diffraction-free waves [5]. The elementary nondiffracting beams are, therefore, often referred to as Bessel beams.

Independently of all these theoretical considerations, Bessel-like beams had also been produced already in the 50's by McLeod with the use of conical axicons [6, 7]. They were not considered nondiffracting at the time although they were known to produce a continuous line of images from small sources. Kelly was also able to show that their radial pattern is described by the zeroth-order Bessel function [8]. Apparently nearly unknown to the western-world physicists (times have changed a lot since then) Bunkin & *al.* had in the 80's in Moscow used an axicon to produce 'continuous laser sparks' from Gaussian laser beams *with a 1 GW laser (peak) power* [9, 10]. In the West in 1989, Indebetouw suggested, based on the McCutchen theorem [11], that an axicon could be used to form a Bessel beam [12] and this was later experimentally realised by Scott and McArdle [13].

The Acoustics society was also interested in studying Bessel beams and the first ultrasonic transducer was fabricated by Hsu & *al.* in 1989 [14]. The application potential of nondiffracting waves was soon understood in high-resolution medical imaging [15]. A whole new research line was, however, initiated by Lu and Greenleaf with the realisation that the nondiffracting Bessel beams could be generalised into nondiffracting pulses called X waves [16]. In spite of a very simple principle, namely that all frequency components must propagate at the same angle with respect to the propagation axis [17], such pulses would have been difficult to produce in optics where simultane-

ous, coherent control is very complicated over a wide range of frequency components. This was, however, later achieved by Saari and Reivelt in 1997 [18]. With acoustic transducers it was hardly more difficult than with continuous-wave Bessel beams.

Many theoretical and practical questions associated with Bessel beams and X waves have been addressed since. Most importantly, mathematically ideal waves inevitably had properties that appeared unphysical: both wave types required an aperture of infinite extent and also an infinite amount of energy [19]. Bizarrely, X waves also seemed to propagate with a superluminal velocity [16]. The latter 'problem' was solved by understanding that the energy (or information) carried by the X wave was *not*, in fact, carried by the central pulse but it was, instead, launched at some previous time from outer regions of the aperture, thus having exactly enough time to propagate at the speed of light. The truncation of the infinite aperture has, by now, turned into an engineering-type question of how the truncation should be best done in order to avoid unnecessary ripples or edge diffractions within the desired finite propagation length.

During the ten years subsequent to the discovery of the X waves, localised non-diffracting pulses have been studied extensively. Again, however, these wave solutions had their predecessors. In 1983, Brittingham had published the discovery of 'focus wave modes' that are pulse-like waves propagating in three dimensions with the speed of light [20]. They had the peculiar property of remaining focused at all times, i.e., their spatial envelope did not change under propagation, although the pulse within evolved periodically. Thus, they were considered nondispersive. The original, rather cumbersome formulation of focus wave modes was generalised by Sezginer who also showed that no focus wave modes of finite energy can exist in free space without sources [21]. Although focus wave modes and X waves are clearly different kinds of waves, they have very similar spectral properties, as was pointed out by Shaarawi [22]. This suggests that they both belong to a larger class of localised waves. A theory of 'diffraction-free pulses at arbitrary speeds' has been presented in one of the papers constituting this thesis [I]. Such waves comprise X waves as a special case of superluminal pulses and focus wave modes as a case of luminal waves.

The pulse-like waves, such as X waves have reached general, albeit mainly academic interest. Bessel beams, on the other hand, have shown application potential in several fields. Their long and narrow focal line suggests good lateral resolution in imaging applications and it has been the driving motivation for the nondiffracting waves research in medical imaging; see, for instance [23] and references therein. The depth of focus and the good transverse resolution of the focal line have also proven to be advantageous in optical microlithography [24] and Bessel beams have also been considered for improving the heterodyne detection efficiency [25]. Especially wide has been the interest in using

Bessel beams in second- and higher-order harmonic generation in nonlinear optics [26]. This is due to the ease in tuning the axial wavelength of the Bessel beam in order to meet the phase-matching criteria [27, 28]. Several other fields of applications have recently also been considered, such as the manipulation of microscopic particles [29].

At present, the field of nondiffracting waves appears to have reached a state of certain maturity: the novel and surprising properties of both Bessel beams and X waves are now well understood and the main emphasis of research has moved into both scientific and industrial applications. Nondiffracting waves, as such, remain rather straightforward solutions to the linear wave equation. Their speciality and usefulness lies in their focusing and tuning properties that can advantageously be used in other fields of physics and engineering sciences as well.

2 Periodically propagating waves

The discovery of propagation-invariant beams naturally led to the idea of similar pulses or wave packets. Solitons are, of course, well-known for waves propagating in nonlinear media where the nonlinearity serves to counterbalance the effect of diffraction. Similarly (radial) changes in the index of refraction can be used to form a waveguide that supports localised waves. In free space or in a linear medium, no such counterforces are available.

Bessel beams can, however, be used to build up wave packets that retain the r^{-1} intensity localisation inherent to the Bessel functions of the first kind. The key feature of localised pulses is the strict spatio-temporal coupling that may yet take several different forms, leading to different classes of localised pulses; X waves [16] are the most natural in the sense that they are strictly propagation-invariant. They are also bound to have superluminal propagation velocities. If a periodical propagation invariance is allowed, wave packets can be constructed for arbitrary velocities [I]. A special class of these, on their own importance, are focus-wave modes that propagate at the speed of light [20]; similar waves also exist for subluminal velocities [II].

2.1 Bessel beams

Before proceeding to more general wave-forms, Bessel beams need to be discussed briefly since they are the main constituents of all localised diffraction-free waves in three dimensions.

The simplest of all nondiffracting waves, i.e., the radially symmetric fundamental Bessel beam, has the mathematical form [19]

$$J_0(k_\perp r)e^{\mathrm{i}(k_z z-\omega t)}, \tag{2.1}$$

where r is the cylindrical radial coordinate and z is the coordinate along the optical axis. The radial and the axial wave vectors, $k_\perp = (\omega/c)\sin\zeta$ and $k_z = (\omega/c)\cos\zeta$, respectively, are determined through the cone angle ζ that defines the direction of (phase) propagation with respect to the optical axis. Hence the angular spectrum of the nondiffracting wave is bound to a circle of radius $k_\perp$ in the Fourier space [12]; this can be clearly observed from a phase-sensitive measurement of a millimetre-wave beam in figure 2.1.

The central beam, i.e., the focal line of the Bessel beam appears to propagate indefinitely without any diffractive spreading. The entire beam also, unavoidably, contains side lobes whose intensity envelope decreases as r^{-1} when moving away from the optical axis. This exponent has an entirely geometrical origin: the energy is radiated towards

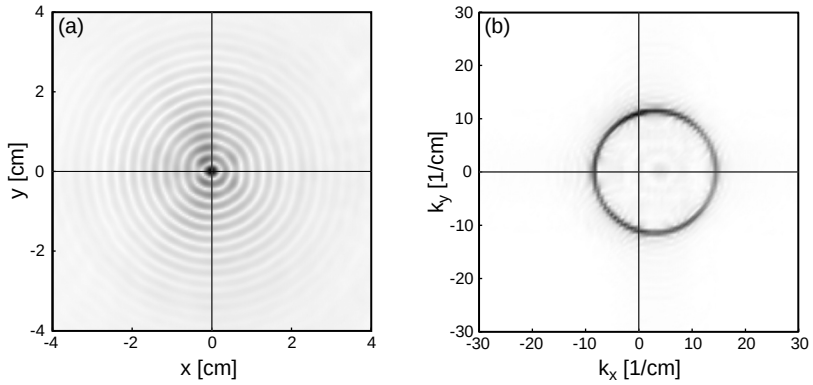

Figure 2.1: Measured radio-frequency Bessel beam, published in [VIII]. (a) Absolute value of Bessel beam amplitude. (b) Fourier transform of the complex-valued beam measured. The latter is confined in the vicinity of a circle of radius $k_\perp = 11$ cm^{-1}. The displacement from the Fourier-space origin is attributed to a 2.75° misalignment of the measurement plane. The wavelength is 0.96 mm.

the axis along the cone shell illustrated in figure 2.2; an equal energy flux is carried through each cross section of the cone shell and the flux density (intensity) is therefore inversely proportional to the cross-sectional area[4].

As the cone of energy propagation in figure 2.2 suggests, there exists a wave component that carries energy towards the optical axis; this wave is necessarily singular since the energy carried by such a wave component vanishes once it reaches the axis [31]. On the other hand, another wave carries energy away from the axis and these two can be expressed in terms of the second and the first Hankel functions, respectively. They cancel each other's singularities and their superposition yields the physical Bessel beam. The evolution of an apertured Bessel beam into a Hankel beam of the first kind can be observed in figure 1.1 and also in figure 4.4 below in section 4.2.2. At the Bessel beam waist the two Hankel beams are in complete balance; the oscillatory radial form of the Bessel beam is due to the standing-wave interference pattern of inward and outword propagating components. Due to the conical energy propagation, the Bessel beams' ability of energy transport is very different from that of ordinary Gaussian beams [32, 33, 34].

Nondiffracting beams are generally defined as beams of which the transverse (intensity) pattern remains invariant along the beams axis. The zeroth-order Bessel beam is the only axisymmetric beam with no azimuthal energy flux. The higher-order Bessel

[4]No *localised* nondiffracting waves exist in two dimensions since the cone shell area in two dimensions is independent of the distance from the axis [30].

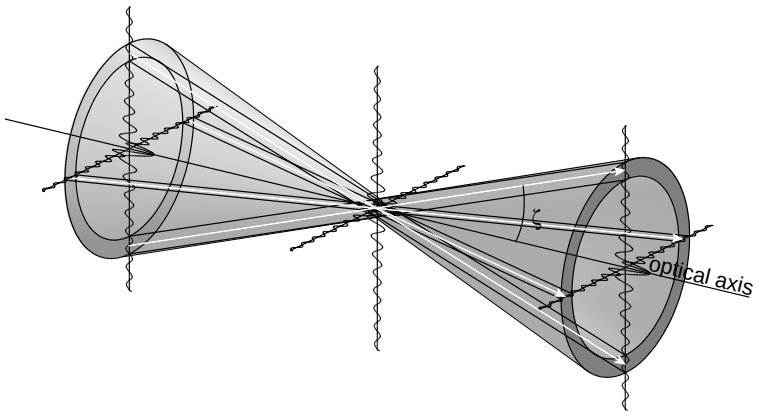

Figure 2.2: Energy propagation within the zeroth-order Bessel beam. The long white arrows indicate energy propagation along the cone shell.

functions are, however, known to provide similar waves [3, 4], and the most general nondiffracting waves are obtained as superpositions of different orders as [12]

$$\sum_{n=-\infty}^{\infty} p_n e^{\mathrm{i}n\varphi} J_n(k_\perp r) e^{\mathrm{i}(k_z z - \omega t)}, \tag{2.2}$$

where p_n are the weights of the superposition and φ is the azimuthal angle in the (x, y)-plane. Individual higher-order beams carry the topological charge n due to a phase singularity at the origin; consequently, their amplitude necessarily vanishes along the optical axis so as to preserve continuity. Hence they can be called rotating or spiral nondiffracting beams [35] with optical vortices [36] and they also carry orbital angular momentum [37].

2.2 Periodic wave modes

Periodically propagating waves are not strictly propagation-invariant although they avoid diffractive spreading by returning to their original pattern after a certain propagation distance or time. They are further allowed to rotate in-between. A systematic approach has been introduced in [I] for all periodically evolving pulsed waves for velocities $0 < v < \infty$. Their spectral characteristics vary according to whether this velocity of propagation equals, exceeds, or is below the speed of light.

Rotationally periodic waves (RPWs) comprise beams and pulses whose amplitudes evolve periodically along an infinite screw curve shown in figure 2.3. After a time elapse τ, the wave has propagated the distance $\xi = v\tau$ along z, simultaneously rotating

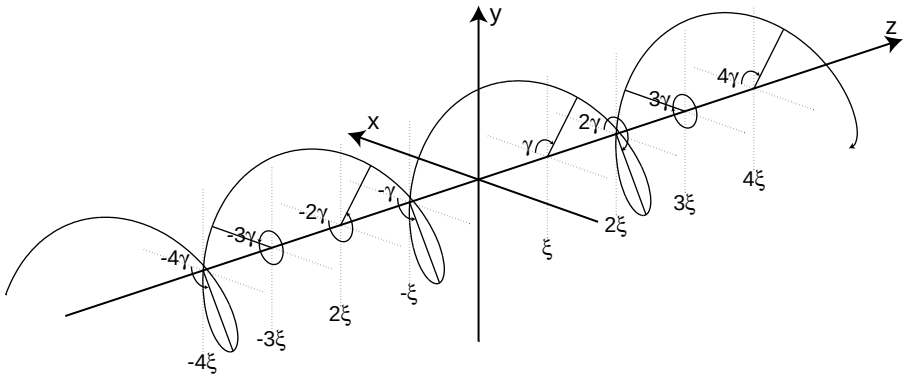

Figure 2.3: Periodic wave amplitude is required to regain its initial value at multiples of the pitch ξ along the screw curve. Here $\gamma = 2\pi/3$.

through the angle γ and, finally, recovered its original amplitude pattern [38]. The ratio of the axial distance and the time lapse is the velocity of propagation, $v = \xi/\tau$. Mathematically, the wave field obeys the condition

$$\Phi(r, \varphi + \gamma, z + \xi; t + \tau) = \Phi(r, \varphi, z; t), \tag{2.3}$$

together with the unique-valuedness condition

$$\Phi(r, \varphi + 2\pi, z; t) = \Phi(r, \varphi, z; t). \tag{2.4}$$

The wave mode is assumed to satisfy the standard wave equation

$$\nabla^2 \Phi = \frac{1}{c^2} \frac{\partial^2}{\partial t^2} \Phi \tag{2.5}$$

throughout the space, and hence it may be represented, for instance, as a superposition of plane waves

$$\phi = e^{\mathrm{i}(k_x x + k_y y + k_z z - \omega t)} \tag{2.6}$$

that satisfy the dispersion relation $k_x^2 + k_y^2 + k_z^2 = \omega^2/c^2$. Here ω is the temporal Fourier (angular) frequency and it may also assume negative values. Equivalently, in cylindrical coordinates that are a natural choice for rotation, waves can also be expressed in terms of Bessel beams

$$\phi = e^{\mathrm{i}n\varphi} J_n(k_\perp r) e^{\mathrm{i}(k_z z - \omega t)} \tag{2.7}$$

whose dispersion relation states $k_\perp^2 + k_z^2 = \omega^2/c^2$.

Using the Bessel-beam representation of the wave that satisfies the conditions given by equations (2.3) and (2.4), a further restriction is obtained for k_z, namely

$$k_{z,ln} = \frac{\omega}{v} + \frac{2\pi l - n\gamma}{\xi} \equiv \frac{\omega}{v} + \mu, \tag{2.8}$$

where l and n are arbitrary integers. They may be interpreted to be associated with the field properties along the screw curve in figure 2.3 and on the rotations for constant z, respectively. Subsequantly, the axial wave number is also uniquely determined through

$$k_{\perp,nl} = \sqrt{\frac{\omega^2}{c^2} - k_{z,ln}^2}. \tag{2.9}$$

Two comments are in order concerning the above result: (i) It is a spectral extension of that derived in [38] for monochromatic *generalised propagation-invariant wave fields*. The essential difference is that the constant term common to all l and n in equation (2.8) is linear in frequency ω, resulting in a definite propagation velocity[5]. (ii) Both X waves and focus-wave modes are characterised with a similar coupling between the temporal frequency and the axial (and radial) wave numbers [39]. In fact, they are both shown to arise as special cases of the rotationally periodic waves.

Although waves determined by equations (2.8) and (2.9) are perfectly acceptable free-space solutions of the wave equations, they suffer from several drawbacks. The velocity of propagation is here implicitly assumed positive and hence the wave on the whole propagates along positive z. If the wave concerned is intended to be excited with a planar aperture, all its Bessel-beam constituents must also carry energy along positive z so as to satisfy the Sommerfeld radiation condition [40]. For a positive (negative) angular frequency, this also requires a positive (negative) wave number k_z; yet this is by no means guaranteed by the dispersion relation involved. This criterion of causality is known to cause problems for focus-wave modes [41]. Limiting the frequency further to those ω that satisfy

$$\frac{k_z}{\omega} > 0 \tag{2.10}$$

allows the wave field to be causally excited using a planar aperture.

Another problem arises from the spatial extent of the aperture. The amplitudes of periodic waves are only localised as $r^{-1/2}$ and, as time goes on, the excitation is needed for arbitrarily large values of r. If the temporal aperture is bounded, the wave field generated will retain it periodic form only for a finite length of propagation.

[5] As mentioned in [I], this velocity of propagation sometimes becomes ambiguous for monochromatic fields.

The Fourier representation of the wave field in real space now has the form

$$\Phi(r,\varphi,z;t) = \sum_{l,n} \Big[e^{\mathrm{i}[n\varphi+(2\pi l-\gamma n)z/\xi]} \times \int a_{ln}(\omega) J_n(r k_{\perp,ln}) e^{\mathrm{i}\omega(z/v-t)} \mathrm{d}\omega \Big], \tag{2.11}$$

where the frequency ranges in the integrals are individually limited, depending on l and n. This representation is characteristic to all localised pulses: The wave is decomposed into *single-mode waves*, of which the envelopes propagate with the predefined velocity of propagation v; the periodicity properties required are fulfilled with the phase factor. The dispersion relation for rotationally periodic waves, given by equation (2.8), fixes the radial and the axial wave numbers uniquely to the frequency and the remaining degree of freedom is the Fourier spectrum given by $a_{ln}(\omega)$.

Mathematically, no constrains were imposed on the shape of the propagating wave field. The requirement of periodic propagation, with or without rotation, leads to the axial dispersion relation for each mode, given by equation (2.8). However, the resultant fields, especially for single-mode waves with fixed l and n, feature clear wave-front structure. This is due to the single-valued dependence of both the axial and radial wave numbers on frequency since, consequently, each frequency has a dominant direction of energy propagation, given by the group velocity.

While the pulse centre moves along the optical axis, it is, in fact, all the time reconstructed by the wave fronts approaching the axis with the speed of light. The apparent velocity of propagation is only determined through the time elapse between the wave focusing at z and at $z+\xi$, see figure 2.4. Hence the propagation of a localised periodic pulse only arises from a synchronous formation of the focal spot along the optical axis and, consequently, neither energy nor information is actually carried by the pulse itself.

Rotationally periodic waves satisfying a more stringent condition than that given by equation (2.3) can be classified into the following subclasses: *Uniformly propagating waves* carry a constant amplitude along the screw curve, hence they are limited to $l = 0$. *Nondiffracting waves* (or X waves) are further required to propagate linearly with no rotation; they also obey $\gamma = 0$. *Self-imaging waves* recover their form with no rotation, hence they also have $\gamma = 0$ but unlimited values of l. *Rotationally invariant waves* have $n = 0$ and are, consequently, independent of the value of γ. All these wave forms are summarised in table 1.

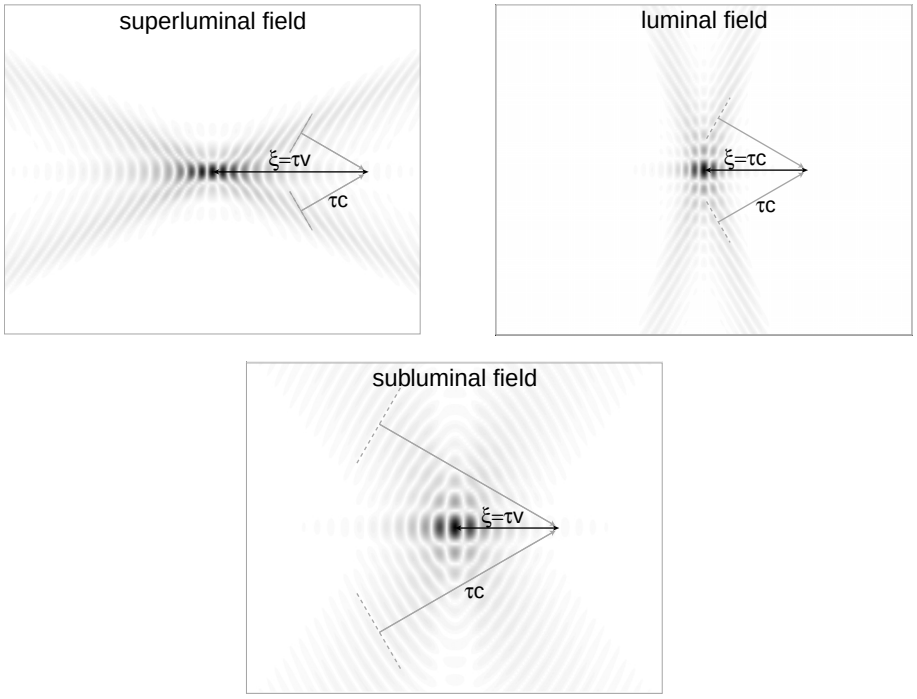

Figure 2.4: Superluminal ($v = 2c$), luminal ($v = c$), and subluminal ($v = c/2$) pulses. Here τ is the time needed for the pulse centre to move the distance ξ along the optical axis. Dashed lines denote local wave fronts that are to constitute the new pulse after the time τ.

2.3 Nondiffracting X waves

Of all periodically propagating waves, X waves are the most widely studied, and they also perhaps constitute the most straightforward generalisation of Bessel beams into localised pulses since, ideally, they propagate uniformly devoid of any changes in their amplitude pattern. Alternatively, as put by their discoverers, *X waves are multiple frequency waves but they are nondiffracting in both transverse and axial directions* [16].

The X waves, similarly to Bessel beams, are characterised by a frequency-independent cone angle ζ that determines the directions of both the phase propagation and the energy flow with respect to the optical axis. Their name owes to the subsequent conical form which, on a meridional place, is seen as an X-shaped intensity pattern, see figure 2.5. The axial and the radial wave numbers satisfy $k_z = \frac{\omega}{c}\cos\zeta$ and $k_\perp = \frac{\omega}{c}\sin\zeta$, respectively. This is, however, only a special case of rotationally periodic waves with $v = c/\cos\zeta$ and $\mu = 0$. The latter condition[6] requires that $l = 0$ and $\gamma = 0$,

[6]The requirement is actually that $\mu = (2\pi l - n\gamma)/\xi = 0$ which also holds for $n = 2\pi l/\gamma$. This is a

Wave type	γ	n	l
General RPWs	free	free	free
Uniformly propagating waves	free	free	$l = 0$
Nondiffracting waves	$\gamma = 0$	free	$l = 0$
Self-imaging waves	$\gamma = 0$	free	free
Rotationally invariant waves	-	$n = 0$	free

Table 1: Classification of different rotationally periodic waves (RPWs). If n is bound to zero, the rotational parameter γ plays no role. Therefore, it is omitted from the rotationally invariant waves.

as indicated in table 1. The X waves can only exist for superluminal propagation velocities since $v = c/\cos\zeta \geq c$; luminal waves with $\mu = 0$ are merely wave packets made out of plane waves that propagate along z, while no subluminal waves may exist for $\mu = 0$.

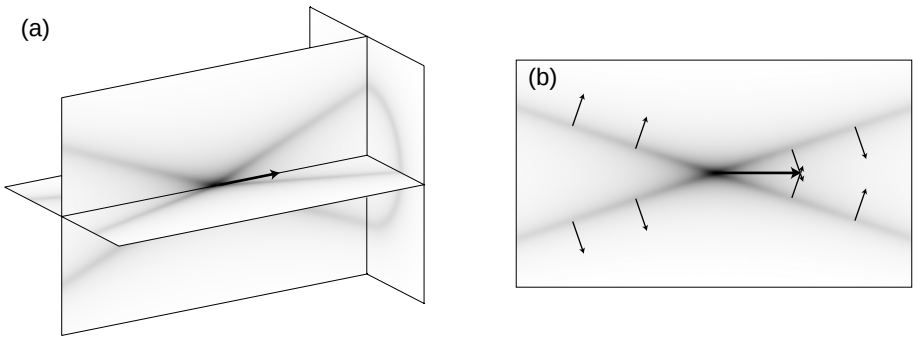

Figure 2.5: (a) Three-dimensional illustration of an X wave. The conical structure of an X wave is *not* the same as in figure 2.2; here energy and the cone propagate along the normal of the cone. (b) X wave in the meridional plane. Small arrows show the propagation of the energy while the large arrow denotes the propagation of the entire wave pattern.

Nondiffracting X waves have a particularly simple mathematical form as a wave

mere redundancy since the actual wave fields are identical, being both periodic along a screw curve *and* constant along a line parallel to the optical axis.

packet of Bessel beams

$$\Phi_X = e^{in\varphi} \int_0^\infty a(\omega) J_n \left(\frac{\omega \sin\zeta}{c} r \right) e^{i\omega(z/v - t)} d\omega, \tag{2.12}$$

where the integral is limited to positive frequencies only (the field itself is described accordingly as a complex-analytic function). The exact spatial shape of the X wave depends on the Fourier frequency spectrum chosen. Effects of the X-wave spectrum are analysed in detail in [III]; a suitable set of spectra can also be used to find an orthogonal set of X waves [IV].

As for Bessel beams, the main characteristic properties of X waves are understood in terms of the scalar theory. The proper electromagnetic treatment of X waves is, nonetheless, sometimes preferred and it can be obtained, for instance, by considering the scalar X wave as a Hertz potential [42]. Vector X waves can also be found by the direct use of vector Bessel beams [43, 44] whose polarization modes [45] are inherited by the corresponding X waves. The situation becomes more complicated in the presence of anisotropy where Bessel beams, themselves, have to be modified.

2.4 Focus-wave modes

Focus-wave modes were perhaps the first localised pulses discovered that are based on Bessel beams although this relation was not noted until later. They were first presented for the transverse electric mode of full Maxwell's equations[7] [20]. The original focus-wave modes were reformulated (and rederived) using a clever choice of variables [21]: $z - ct$ and $z + ct$. The envelope of the wave is allowed to depend only on the former (together with x and y), while the latter only gives rise to a phase factor. This forces the wave envelope to propagate undisturbed along z at the speed of light. The simplest of the focus wave modes is, in fact, a moving (transversely) Gaussian pulse modulated by a plane wave [47]

$$\Phi = e^{ik(z+ct)} \frac{e^{-kr^2/[z_0 + i(z-ct)]}}{4\pi i[z_0 + i(z-ct)]} \tag{2.13}$$

The wave profile at the waist of a general focus wave mode can be determined arbitrarily and it will further fix the entire wave, together with a real parameter used in the phase factor [21]; a complete set of focus-wave modes is obtained with Hermite-Gaussian transverse profile.

[7] This solution was later found to have discontinuities, across which Maxwell's equations were not met [46].

The focus-wave modes also hold a strict connection between the temporal and the spatial spectra; they have been demonstrated to satisfy [48]

$$\omega = \frac{ck_\perp^2}{4\beta} + c\beta, \tag{2.14}$$

where β is a characteristic constant. Using the notation of periodic waves, this is equivalent to a luminal wave with $\mu = -2\beta$. Considering a nonrotating focus-wave mode, this is equivalent to an $l = -1$ mode with the periodic distance $\xi = \pi/\beta$.

Focus-wave modes but suffer from one major problem: they are not necessarily causal or, to be more precise, they cannot necessarily be excited with a planar aperture. As shown explicitly with the simplest of focus waves, it is essentially radiated in the direction opposite compared to the intended direction of pulse propagation [41]. Focus-wave modes do not violate the relativistic causality *in principle* [49], but they contain two parts, one that carries energy along $+z$ and one that carries energy along $-z$. Hence the excitation of a focus-wave mode requires parallel apertures between which the wave can be made to propagate [50]. With the use of the angular-spectrum representation, the two wave components can be treated separately; in fact, a suitable choice of pulse parameters makes the forward-propagating component overly dominant [51].

2.5 Other localised wave modes

Rotationally periodic waves considered above constitute, however, only one variety of localised waves while many others also exist. Although they are not, in principle, within the subject of this thesis, some of them are here described briefly due to their close relations to the rotationally periodic waves.

Pulsed Bessel beams[8] [53] retain their transverse shape since they are constructed in such a way that the radial wave number is independent of frequency. Hence they are naturally generated by all devices that explicitly feature a constant transverse wave number, such as on-axis holograms [54, 55] and acoustic nondiffracting-beam transducers [56]. Their dispersion relation is $k_z(\omega) = \sqrt{(\omega/c)^2 - k_\perp^2}$ (compared with equation (2.8)) and the entire wave factorises into the transverse Bessel-beam distribution and the propagating axial part. The latter, however, is subjected to a 'spatially-induced' group-velocity dispersion due to the nonlinear frequency dependence of the axial wave number.

Acoustic directed-energy pulse trains [47] are constructed from focus wave modes by superposing waves continuously over the free parameter β in equation (2.14). This

[8] Terminology here is not very well established, and the term 'pulsed Bessel beams' has also been used for optical nondiffracting waves [52].

leads to finite-energy pulses that remain essentially invariant over a finite length of propagation. Similar electromagnetic directed-energy pulse trains [57] are obtained using a scalar field (identical to the acoustic field) as a Hertz potential. As a special case, this method yields modified power-spectrum pulses [57].

Paraxial beams and pulses are described using the Fresnel diffraction integral and they can be applied to describe wave propagation, provided that all wave components propagate within a small angle from the optical axis. Bessel-Gauss beams [2] are Bessel beams modified with a Gaussian aperture, which is often a natural choice since Bessel beams are in many cases created using an optical system to transform an incident Gaussian beam into a nondiffracting wave [58, 59]. Bessel-Gauss beams can also be generalised to propagating pulses [60].

The propagation of a Bessel-Gauss beam is twofold: If the Gaussian envelope only covers the central Bessel lobe (or a part of it), the beam is nearly Gaussian and it is dominated by the Gaussian angular spread. For a large Gaussian profile containing several Bessel fringes, the beam appears an apertured Bessel beam dominated by the Bessel cone angle [2] that carries a finite energy flux[9]. On the other hand, standard Laguerre-Gaussian modes can be used to represent *scaling* nondiffracting waves (again, in the paraxial regime) that maintain their spatial form, yet they scale with the enveloping Gaussian beam [62].

[9]Although the Gaussian envelope ensures a finite energy flux within Bessel-Gauss beams, their aperture is still, yet highly localised, infinite in principle. Finite-aperture versions of a plane wave, Gaussian, Bessel-Gauss, and Bessel beams have been analysed numerically in reference [61].

3 Acoustic waves in anisotropic crystals

Research on acoustic (or elastic) waves in piezoelectric crystals is nowadays an important field for several applications, e.g., radio-frequency resonators, band-pass filters, and other microwave devices, see, for instance, a recent survey in reference [63]. Subsequently, new techniques for acoustic-wave imaging have also been developed [64, 65, 66] for experimental research on anisotropic waves in crystals where the lattice strongly influences the acoustic wave propagation. In [V] it is shown that, theoretically, anisotropic crystals can also support nondiffracting wave modes and in [VI] a scheme is presented for the generation of nondiffracting beams with the use of transducers similar to those employed in commercially available acoustic resonators.

Wave propagation in the presence of a strong anisotropy essentially differs from that in isotropic media. The formation of wave fronts may display folds and cusps that are evidence for an energy propagation very much deviated from the direction of phase propagation. In particular, some directions of the crystal lattice are able to focus (divergingly) strong energy fluxes, and they can be observed through the formation of caustics, i.e., directions of singular phonon focusing. Properties of anisotropic wave propagation are naturally described in terms of the slowness- and group-velocity surfaces characteristic to each individual crystal; see, e.g., Refs. [67, 68] and the phonon focusing is a direct consequence of the geometrical curvature of the slowness surface.

Acoustic nondiffracting waves inherit the characteristic properties of the specific anisotropic crystal in which they propagate. Hence their properties can be described with transverse slowness and velocity curves that provide physical insight into their propagation [VI]. Treatment of anisotropic nondiffracting waves is not, however, limited to acoustic waves in crystals; an identical formalism may be used for electromagnetic waves in the presence of birefringence [69].

3.1 Anisotropic wave propagation

Acoustic wave propagation in (linear) anisotropic crystals is described using the anisotropic wave equation [64, 70, 71]

$$\sum_{l,m,n=1}^{3} c_{klmn} \frac{\partial}{\partial x_l} \frac{\partial}{\partial x_n} U_m(x_1, x_2, x_3; t) = \frac{\partial^2}{\partial^2 t} U_k(x_1, x_2, x_3; t), \tag{3.1}$$

where the U_i are the $x = x_1$, $y = x_2$, and $z = x_3$ components of local displacements, c_{klmn} is the stiffness tensor (tensor of elastic moduli) characteristic to the material, and ρ is the mass density. Plane-wave solutions

$$\boldsymbol{u}(\boldsymbol{r}; t) = \boldsymbol{U} e^{\mathrm{i}(\boldsymbol{k}\cdot\boldsymbol{r} - \omega t)}, \tag{3.2}$$

to the above equations are obtained from the Christoffel (eigenvalue) equation

$$\sum_{l,m,n=1}^{3} c_{klmn} k_l k_n U_m = \rho \omega^2 U_k. \tag{3.3}$$

If the material used is piezoelectric, equation (3.3) is further modified by replacing the tensor of elastic moduli with the piezoelectrically stiffened moduli $\tilde{c}_{klmn}$, see reference [71] for details[10].

Since there are three linearly independent directions of displacements in solids, there are also three linearly independent polarizations for plane waves propagating along each direction. Their phase velocities are usually different, and they are often named the longitudinal (L), the fast transverse (FT), and the slow transverse (ST) modes, in the order of decreasing phase velocity. In the presence of a weak anisotropy, their names refer to their dominant polarization components. In nondispersive crystals[11], plane waves are often described using the slowness vectors $\boldsymbol{s} = \boldsymbol{k}/\omega$ instead of wave vectors; the length of the slowness vector equals the inverse phase velocity of the given plane wave. Allowing the direction of the slowness vector to vary freely, the vectors trace three slowness surfaces characteristic to each crystal, see figure 3.1.

Propagation of laterally or temporally limited wave packets is known to be described by the group velocity $\boldsymbol{V} = [\partial\omega/\partial k_x \ \partial\omega/\partial k_y \ \partial\omega/\partial k_z]$ that is a vector normal to the surface spanned by the slowness vectors. Due to nondispersiveness, the wave vector and the group-velocity vector satisfy $\boldsymbol{V} \cdot \boldsymbol{k} = \omega$ or, equivalently, $\boldsymbol{V} \cdot \boldsymbol{s} = 1$. They are not, however, necessarily collinear, as in isotropic media; the group-velocity component along the wave vector equals the phase velocity but it often also contains a transverse component.

The slowness and group-velocity relation causes somewhat surprising phenomena. The slowness surfaces are, in fact, defined such that along a radial direction from origin, the first allowed slowness belongs to the L mode and the two subsequent modes to the FT and ST surfaces, in this order. Although the slowness surfaces are commonly named as the L, FT, and ST modes, they are not necessarily separate from each other. Especially, the transverse modes (that are identical for isotropic waves, except for polarizations) are often in contact with each other and it is possible to move smoothly

[10] The stiffening of the elastic moduli depends on the direction of the wave vector and may hence only be applied to the Christoffel equation and not to the anisotropic wave equation that must be explicitly coupled to the electric potential to include piezoelectric effects.

[11] Acoustic phase velocities in crystals are usually independent of the frequency, provided that the wavelength is much longer than the interatomic separation; acoustic vibrations are therefore considered nondispersive [72].

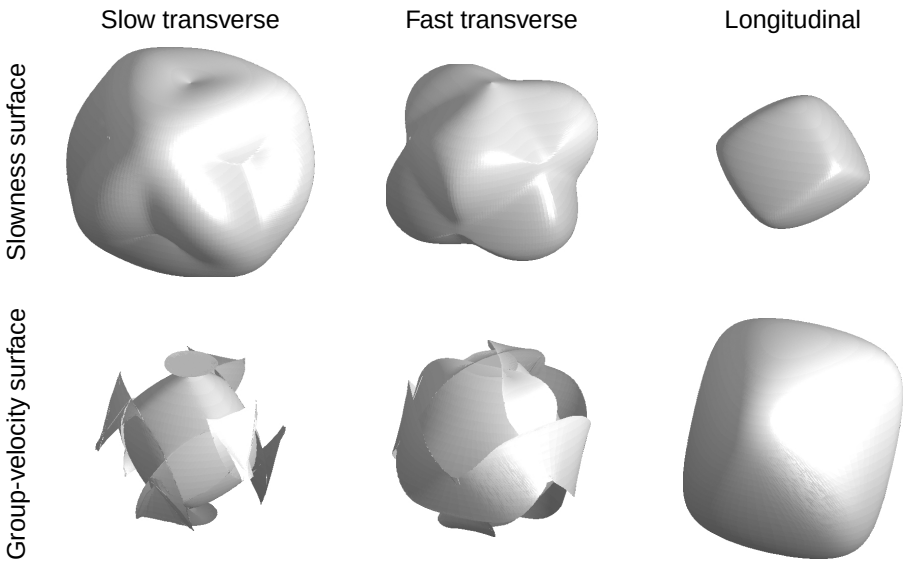

Figure 3.1: Slowness and group-velocity surfaces of quartz. The two transverse surfaces are not actually separate; the sharp tips on the north poles are due to a conical interconnection between the surfaces. The non-convex regions on the two transverse slowness surfaces creates folds on the corresponding group velocities; the longitudinal slowness surface is convex and, consequently, the group-velocity surface is smooth.

from one surface to another, as can be seen in figure 3.1. While the slowness vectors are allowed to move around all directions, the corresponding group-velocity vectors span group-velocity surfaces. Even though the slowness surfaces are smooth[12], the group velocity sometimes develops sharp folds. This is due to the fact that there are possibly several wave modes that propagate energy along the same direction.

The anisotropy of wave motion leads to the following, quite unexpected phenomena, illustrated in figure 3.2:

Beam steering The anisotropic beam-steering effect arises from the fact the group-velocity vector may have a component perpendicular to the wave vector. If an acoustic beam of finite width is generated, predominantly having the wave vector $\boldsymbol{k}$, the beam energy and its cross-sectional envelope actually travel along $\boldsymbol{V}$, thus moving partially sidewise [73]. This effect is, in fact, analogous to dispersive waves where a (temporally)

[12]Slowness surfaces may be taken smooth but this can require joining the surfaces together, such that a smooth movement along one surface continues onto the other on.

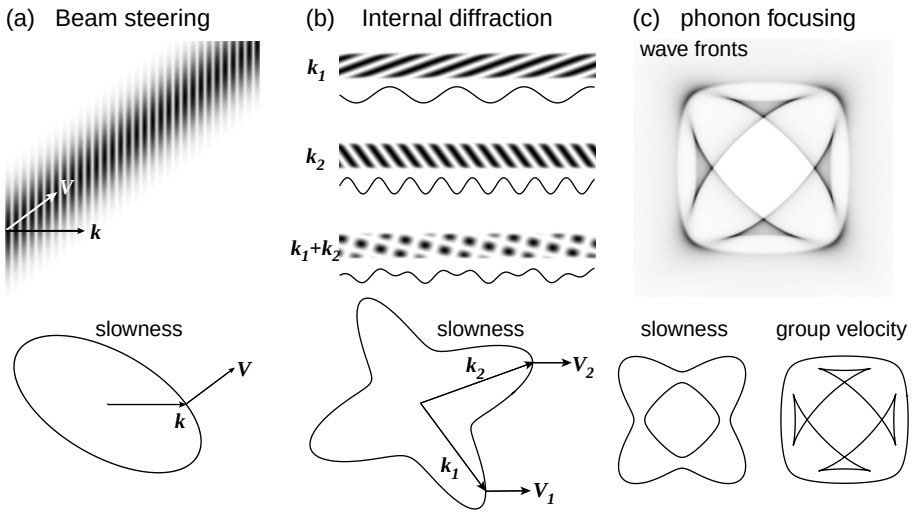

Figure 3.2: Beam steering, internal diffraction and phonon focusing in anisotropic solids, illustrated schematically in 2 dimensions. (a) In beam steering, the beam moves laterally relative to $\boldsymbol{k}$. (b) In internal diffraction, two different wave components propagate to the right and their mutual interference gives rise to an interference pattern. (c) Strong phonon focusing occurs along the diagonal directions of the inner slowness curve, i.e., the outer wave front. Note that the wave fronts have the shapes of the group-velocity curves.

localised wave packet propagates at the group velocity, instead of the phase velocity.

Internal diffraction Internal diffraction is, despite its somewhat misguiding name, an interference effect. If a wave is generated with a time-harmonic perturbation, plane-wave-like oscillations start to propagate along each spatial direction. Along a fixed direction, such waves are observed whose group-velocity vectors point in that direction. If the associated slowness surface is not convex, there may exist several wave vectors that all share a common direction of group velocity, and they are all observed at the same point. Since they have, however, different wave vectors, their superposition displays an interference pattern that is called internal diffraction. If, on the other hand, a wave is launched as an instantaneous pulse, the wave fronts correspond to the expanding group-velocity surfaces. In the latter case, waves moving along the same direction cross the observation point at different times.

Phonon focusing Wave energy in anisotropic crystals is often strongly focused in certain directions relative to the crystal orientation. This effect is observed if the wave is excited with a rather isotropic source that gives rise to equally strong plane-wave components in each $\boldsymbol{k}$ direction. Since the plane waves, however, propagate along $\boldsymbol{V}$, the wave energy concentrates in directions where several $\boldsymbol{k}$-values have a nearly equal $\boldsymbol{V}$. When the curvature vanishes altogether, the energy flux diverges (in the geometrical optics approximation [74]) for an infinitely small point source. This is called a caustic. Physically, all sources have a finite size and integrating over the source region cancels the divergence, yet the relative phonon-flux level can still achieve a value one hundred times larger than the average [68].

3.2 Nondiffracting waves

Just like for ordinary isotropic waves, anisotropic waves are also nondiffracting provided that all the wave components share an equal phase velocity along the beam axis. This prevents the components from mutually dephasing, which would change their interference pattern. In terms of slowness, each wave must have the same slowness along z (the z axis being the beam axis); in figure 3.3 the slowness surfaces have been cut at $s_z = \text{constant}$, the inverse phase velocity along the beam axis. The intersection of a slowness surface with the $s_z = 1/v$ plane is a slowness curve whose geometry already determines the shape of a nondiffracting beam or a pulse. For isotropic waves, this slowness curve is merely a circle as shown in the illustration of a measurement in figure 2.1.

Nondiffracting wave modes are superpositions of plane waves that all satisfy $s_z = 1/v$, i.e., $k_z = \omega/v$,

$$\boldsymbol{u} = \int\int A(\omega,\theta)\boldsymbol{U}(\theta)e^{\mathrm{i}\omega[s_x(\theta)x+s_y(\theta)y+s_z z-t]}\mathrm{d}\theta\mathrm{d}\omega. \tag{3.4}$$

Here the θ-integral extends over one or more slowness curves in the $s_z = 1/v$-cut plane, and the ω integration covers different frequency components. The arbitrary function $A(\omega,\theta)$ represents the weight of each plane-wave component. We choose θ as the arc-length parametrisation of the slowness curve(s) while all other contributions are included in the weight function $A(\omega,\theta)$. The polarization $\boldsymbol{U}(\theta)$ is only defined up to a complex constant factor by the Christoffel equation (3.3), and it should be chosen continuous along the slowness curve, i.e., the integration path. If only a nondiffracting continuous-wave beam is considered, the angular frequency ω assumes a constant value and the corresponding integral can be omitted.

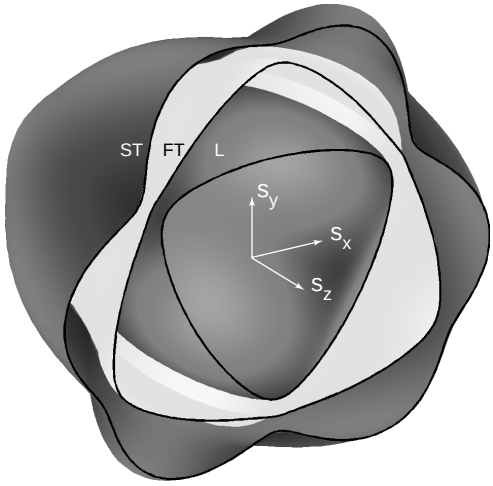

Figure 3.3: Three nested slowness surfaces of crystalline quartz cut along $s_z = 64$ μs/m, i.e., $v = 12.5$ km/s.

On a plane z = constant, a nondiffracting wave appears to behave like a two-dimensional wave[13] whose properties depend solely on the shape of the slowness surface in the $(s_z = 1/v)$-plane. In analogy with ordinary anisotropic waves in three dimensions, a radial velocity $\boldsymbol{V}_\perp$ can be defined that is normal to a slowness curve and also satisfies $V_{\perp x}s_x + V_{\perp y}s_y = 1$. Hence it essentially acts like a group velocity, though it does not describe actual energy propagation. A radial velocity curve is produced corresponding to the slowness curve, and it directly yields the shape of the nondiffracting wave in the (x, y)-plane, see figures 3.4 and 3.5.

More insight into the structure of nondiffracting waves is obtained by studying the asymptotic form of the wave [VI]. Although the wave is globally a superposition of plane waves with a common s_z, it turns out that, away from the axis, only those wave components that carry energy directly towards the axis or away from it locally contribute to the wave pattern. The above-mentioned radial wave-front velocity is, in fact, obtained using this approach. This expansion also reveals the effects of internal diffraction and phonon focusing. If the slowness surface is not convex there are, again, several plane waves to move along the same radial direction and that may interfere, causing internal diffraction. The phonon focusing also becomes explicit since the amplitudes of a plane-wave component not only depend on the weight $A(\theta)$ but also on

[13]This is indeed an anisotropic variant of the fact that an arbitrary two-dimensional wave solution has a one-to-one correspondence with a nondiffracting solution in three dimensions; the time dependence of the former is effectively changed to a $(z\cos\zeta/c - t)$-dependence of the latter, together with a radial scaling $r \to r\sin\zeta$ [75]. Hence the propagation along z appears trivial for ideal nondiffracting waves.

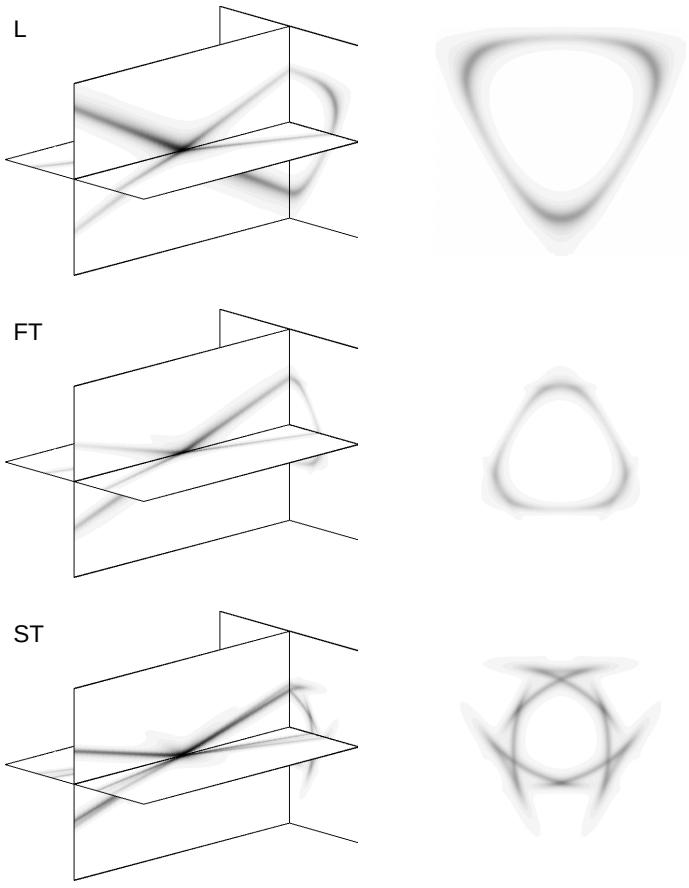

Figure 3.4: Longitudinal (L), fast transverse (FT), and slow transverse (ST) pulse modes in quartz. (left) Three-dimensional shape of the propagating pulse, (right) their approaching cross sections (back planes in left, $z > vt$). Both pulses correspond to the slowness cuts in figure 3.3. The cross sections are directly obtained from the radial-velocity curves in figure 3.5.

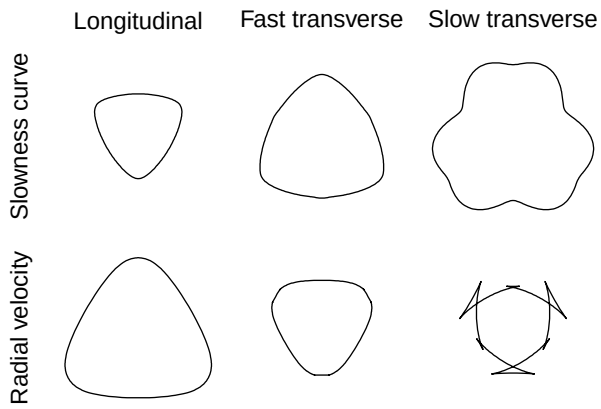

Figure 3.5: Three slowness curves and the corresponding radial velocity curves for quartz. Only the ST mode has a nonconvex slowness and, consequently, its velocity curve exhibits folds associated with wave front caustics. The radial velocity curves readily provide the drifting cross sections ($z < vt$); the approaching cross sections in figure 3.4 are obtained after inversion ($x \to -x$, $y \to -y$).

the inverse square root of the slowness curvature. Consequently, phonons concentrate along the directions of the locally flat slowness surface.

3.2.1 Generation of anisotropic NDWs

The existence and propagation of nondiffracting acoustic waves in anisotropic crystals can be conceived in terms of the slowness surface and plane-wave superposition. An intuitive understanding of the energy propagation associated is further obtained using the asymptotics of the waves where only a few plane waves locally constitute the wave pattern. Physical generation of such waves yet gives rise to several problems that impede experiments on nondiffracting waves. At the time of writing, anisotropic nondiffracting waves have not yet been produced or measured in crystals, to the best of my knowledge. Hence, a means of their excitation and detection is proposed here and it is also discussed in [VI].

A well-established method of wave generation in piezoelectric crystals is the use of electric transducers laid on one of the crystal surfaces. Interdigital transducers, in particular, have been widely studied due to their important applications in microwave filter technology. Interdigital transducers are periodic (or, sometimes, quasi-periodic) linear arrays of metallised strips onto which a radio-frequency current is driven. Due to the piezoelectric effect, the oscillating electric potential excites acoustic waves for

which the period on the surface is determined by the period of the transducer. Interdigital transducers are almost exclusively applied for producing surface-acoustic waves although they can also transmit bulk waves (see, for instance, references [76, 77], and the brief discussion in the Appendix F of reference [78]). While surface waves attenuate exponentially inside the crystal, hence preventing wave energy from leaking away from the transducer [79], bulk waves generated are, essentially, plane waves that propagate into the depth of the crystal.

Similar transducers can be conceived of also being capable for producing nondiffracting beams. Since, asymptotically, only a few wave components essentially contribute along each radial direction, a piezoelectric transducer should be designed to excite these particular waves. This idea is strongly analogous to the use of diffractive elements (computer-generated holograms) in optics to form nondiffracting waves [54]: Hankel beams locally appear like plane waves and they are known to transform into Bessel beams after a certain distance of propagation. Hence it suffices to produce their correct transverse periodicity, i.e., the transverse wave number $k_\perp$, on the surface of the hologram/transducer that, consequently, also determines the axial wave number k_z.

Nondiffracting-wave transducers are, however, in many respects far more complicated than ordinary linear interdigital transducers or diffractive elements and they need to be carefully designed. One of the main problems is that, generally, a periodic transducer creates six different plane waves instead of the one intended. This is due to the existence of the three polarization modes (L, FT, and ST), and all these occur both along $k_\perp$ and $-k_\perp$. Sometimes even the multiples of radial wave vectors appear if the corresponding wave components are not evanescent. A complicated transducer with several elements within one period is likely to allow the exclusion of some of these; another alternative is to design the transducer such that the spurious extra modes do not overlap with the desired beam in the region were they are detected. This leads to a stringent aperture optimisation, see figure 3.6.

Nondiffracting waves propagating within a crystal are most naturally detected on one of the crystal surfaces. The actual nondiffracting beam generated by the transducer in figure 3.6 is merely the central circular spot on the opposite surface of the crystal. Interferometric scanning can be used to measure oscillations along the surface normal with a lateral xy-resolution ≈ 1 μm and an amplitude threshold ≈ 0.1 nm [65, 80].

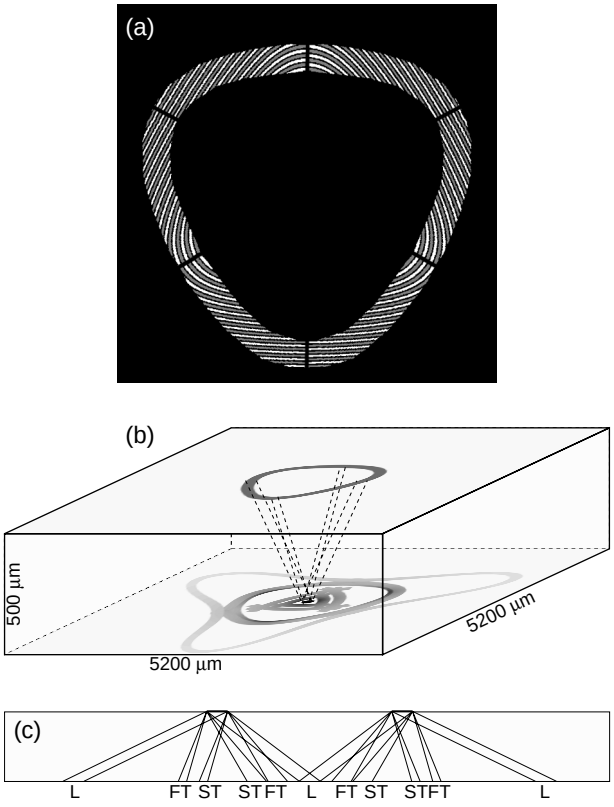

Figure 3.6: Sketch of an aperture-optimised transducer for exciting an L-mode nondiffracting beam in quartz with $s_z = -64$ μs/m (the direction of wave propagation is along negative z). (a) Transducer structure: white denotes grounded electrodes and gray the driving electrodes (bondings must be supplied separetely). The length of the local transducer period scales with inverse frequency, while the shape of the aperture only depends on the intended spot size. (b) The transducer is fabricated on the top surface of the crystal and the wave field generated can be observed on the bottom surface. Several spurious modes are observed in addition to the intended nondiffracting L-mode spot in the centre. (c) Origin of the spurious modes. At each location, the transducer produces two counter-propagating L, FT, and ST modes that all propagate in the direction of the corresponding group-velocity vector.

4 Radio-hologram techniques

Holograms, in the original sense introduced by Gabor in 1948 [81], are photographic plates capable of recording the entire single-frequency optical field, including its phase, superposed with a coherent reference beam. Holography used to refer to the reconstruction of the wave front when the hologram was illuminated with a beam similar to the original reference beam. The observed light field is a reproduction of the original image, created by diffraction from the grating pattern on the holographic film. The computational power developed in the 60's and 70's allowed the numerical synthesis of holograms that were used to construct wave fields without any 'original' images; the grating pattern on the hologram was designed numerically to transform the incident wave field into the desired field [82]. These were called computer-generated holograms, or diffractive optical elements.

The use of radio holograms, i.e., computer-generated holograms in the radio-wave frequencies, began in the 1990's with the primary application of transforming a Gaussian radio beam into a plane wave, to be used in a compact antenna test range (CATR) at 119 GHz [83, 84]. Optical holograms have provided one of the most important methods for producing Bessel beams [54]. Within this thesis, radio holograms have been synthesised to experimentally study the generation and propagation of nondiffracting radio-frequency waves [VII] and other beam-forms [VIII]. Although holograms usually provide smaller efficiencies than instruments used in refractive optics, such as lenses and axicons[14], they allow for more complex shaping of the transmitted beams. High-order Bessel beams were indeed first produced with holograms [55] and highly-refined polarization gratings have recently been shown to be capable of generating Bessel beams of different polarization states [86].

Radio waves have one particular advantage in comparison with optical measurements, namely that it is rather straightforward to measure the *phase* of the field propagating, in addition to its amplitude or intensity. In the optical regime, this is only achieved with complicated interferometric instruments. The existence of the phase information allows detailed analysis of the wave field measured, such as the study of the angular spectrum already illustrated in figure 2.1 in section 2.1.

4.1 Diffractive elements

The function of a (thin) radio hologram is described in terms of a complex-valued transmittance $T(x, y)$ that relates the incident electromagnetic field to the transmitted

[14]Radio-wave Bessel beams have also been produced with axicons [85].

field through

$$E_{\mathrm{tr}}(x,y) = T(x,y)E_{\mathrm{inc}}(x,y). \tag{4.1}$$

This form implicitly assumes that the polarization of both fields is the same, and often it is taken to be linear and constant across the entire hologram. Two stages must be addressed in the hologram synthesis: (i) finding the proper transmittance required for the construction of the desired field and (ii) designing a hologram structure that produces it. A nonamplifying hologram is bound to $|T| \leq 1$; this is, however, often an artificially high upper bound, as will be noted below.

Two types of holograms are usually studied separately. *Amplitude holograms* operate based on the reflection or attenuation of the transmitted field, with no explicit modulation of the phase. The amplitude holograms fabricated here consist of a dielectric mylar film covered with a copper layer, onto which the hologram pattern is etched. The copper layer acts as an ideal conductor, effectively reflecting all the incident field. This allows, within the limits of scalar diffraction theory, a binary amplitude modulation of the transmitted beam[15]. Hologram structures are often locally periodic and, consequently, the beam is diffracted into several distinct diffraction orders; the first order is here used for the desired beam. According to scalar theory, the maximum transmittance obtained is bound to $|T_1| \leq 1/\pi$ although the actual value may be slightly larger when rigorous electromagnetic theory is used.

Phase holograms are made of dielectric material alone and their operation is based on the phase modulation of the beam transmitted. We have used both the commercial material Obomodulan$^{(\mathrm{R})}$ (designed for high-quality milling) and Teflon; the hologram pattern is milled on the surface of a substrate plate. By varying the thickness of the plate locally, the optical length of the field within is changed, introducing local changes in the phase of the beam. Once again, the first diffraction order is used and the transmittance is limited to $|T_1| \leq 2/\pi$. Higher efficiencies compared with the amplitude holograms are usually obtained since no field is necessarily blocked or reflected by the phase hologram[16].

4.1.1 Choosing the desired transmittance

There are several alternatives for how to obtain the desired transmittance function $T(x,y)$ or, equivalently, the desired transmitted electromagnetic field. Two methods

[15] Finite thickness of the holograms, however, deteriorates the pure binary modulation and the actual effect of the hologram must be found using more precise methods.

[16] Some reflections always occur on a dielectric surface but this is often a minor effect in comparison to the reflections caused by an amplitude hologram.

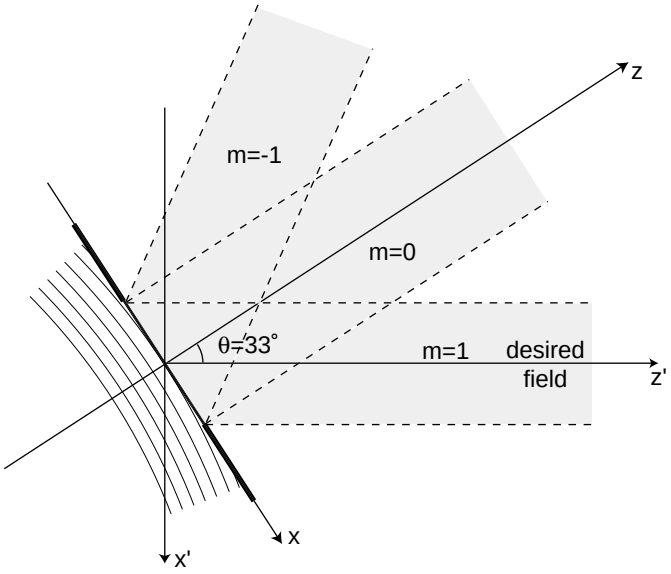

Figure 4.1: Schematic of the radio-hologram geometry. The beam desired is produced in the $m = 1$ diffraction order, 33° from the hologram normal, the angle being chosen such that only the $m = 0$ and $m = \pm 1$ orders are formed. Once the three beams have separated, the desired $m = 1$ beam may be shaped by the hologram optimisation. The boundary diffractions have been excluded here.

are considered here briefly: inspection (sometimes very practical) and back propagation.

If the desired beam form is simple enough, the transmittance may be obtained through inspection. If the hologram is designed to form a plane wave that propagates along z' (see figure 4.1 for the convention of coordinates), the desired beam is

$$E_{\mathrm{tr}} = Ae^{\mathrm{i}kz'} = Ae^{\mathrm{i}k(x\sin\theta + z\cos\theta)}\Big|_{z=0} = Ae^{\mathrm{i}kx\sin\theta}, \tag{4.2}$$

where A is a constant amplitude (see below) and the above expression is the field on the hologram surface. Hence the transmittance needed is obtained from $T(x, y) = E_{\mathrm{tr}}(x, y)/E_{\mathrm{inc}}(x, y)$, where the incident field is assumed to be known. There are two issues that have to be considered here. The field is produced in the first diffraction order (defined through the angle θ) and the constant amplitude must not exceed its efficiency. Using binary quantized amplitude and phase holograms, these limits are approximately $A \lesssim 1/\pi$ and $A \lesssim 2/\pi$, respectively. The hologram also necessarily has a finite aperture whose boundaries limit the field produced. To avoid perturbations

caused by a sharp boundary, the edges must be tapered to allow a smooth decrease of the amplitude to zero. The beam quality is nonetheless bound to deteriorate for large distances.

This simple approach, however, fails for Bessel-beam holograms. Binarisation algorithms often assume that the transmitted field locally behaves like a plane wave; Bessel beams are, effectively, superpositions of two counter-propagating plane waves, which is a much more complicated situation. This would not necessarily be a problem for on-axis holograms that use the zeroth diffraction order, but it complicates the off-axis holograms employed. A Bessel-beam field can nevertheless be obtained if the Bessel-function profile is replaced with the second Hankel function [31] that corresponds to a conical wave that approaches the optical axis, i.e., the z'-axis, in the cone angle ζ. Once it crosses the axis, the beam is changed to the outward-propagating first Hankel function and their mutual superposition is the Bessel beam desired. The divergence of the Hankel beams generated is easily removed on the optical axis by replacing the Hankel functions further with their asymptotic expansions far from the origin, modified such that their amplitude remains finite[17]. The maximum amplitude and the boundaries must be handled similarly as in the above case of the plane waves.

If the field to be produced is only defined at a certain finite distance L from the hologram along the direction of the first diffraction order, the field on the hologram must be found by back-propagating the field onto the hologram. This method also has the advantage of directly handling the boundary effects: the final boundary is determined by the back-propagated field[18]. If the electric field at $z' = L$ is given by $E(x', y', z' = L)$ and its Fourier transform is $\tilde{E}_{z'=L}(k_x, k_y)$, the field at an arbitrary point is obtained using the angular spectrum [40]:

$$E(x', y', z') = \frac{1}{2\pi} \int \left[\tilde{E}_{z'=L}(k_x, k_y) e^{\mathrm{i}\sqrt{k^2 - k_x^2 - k_y^2}(z'-L)} \right] e^{\mathrm{i}(k_x x + k_y y)} \mathrm{d}k_x \mathrm{d}k_y. \tag{4.3}$$

Inserting here the hologram coordinates $x' = x\cos\theta$, $y' = y$ and $z' = x\sin\theta$, the field transmitted by the hologram is obtained. This operation can be evaluated quite efficiently with the use of FFT algorithms.

The back-propagation scheme can be used, for instance, to reduce boundary effects. Radio holograms used for antenna testing are required to produce a high-quality plane

[17] This causes only minor perturbations on the field since, in any case, the field near the optical axis would not behave locally like a plane wave. Secondly, point-like (or small) defects create spherical perturbation whose amplitude decreases in proportion to the inverse of distance.

[18] Actually, the aperture is to be defined, for instance, where the transmitted amplitude drops to 1% of the maximum, which limit may further be tapered.

wave over the area of the receiving antenna[19]. Hence the field at $z' = L$ is to be a plane wave of constant amplitude and phase, tapered to vanish smoothly outside a disc of a certain radius. This field is then propagated back onto the hologram in order to find the transmitted field required. The resulting field is no longer a tapered plane wave but it has diffractive phase and amplitude variations. These, however, should exactly cancel once the field propagates from the hologram to the plane $z' = L$. Much more complicated holograms can also be designed using back propagation, such as the one producing a radio field shaped in the form of the characters 'HUT', see section 4.2.3.

4.1.2 Quantisation of the hologram structure

Hologram quantisation schemes are usually based on the assumption that both the incident field E_{inc} and the transmitted field E_{inc} vary slowly, except for a linear phase on the hologram surface. This is equivalent to assuming near (x_0, y_0) an incident wave of the form $E_{\text{inc}} = E_1 e^{\mathrm{i}[k_{1x}(x-x_0)+k_{1y}(y-y_0)]}$ and a transmitted wave of the form $E_{\text{tr}} = E_2 e^{\mathrm{i}[k_{2x}(x-x_0)+k_{2y}(y-y_0)]}$. Using the abbreviations $k_x = k_{2x} - k_{1x}$, $k_y = k_{2y} - k_{1y}$, and $k_\perp = \sqrt{k_x^2 + k_y^2}$, the rotation angle $\cos\theta = k_x/k_\perp$ (hence $\sin\theta = -k_y/k_\perp$), and local grating coordinates $x - x_0 = \xi\cos\theta + \eta\sin\theta$ and $y - y_0 = -\xi\sin\theta + \eta\cos\theta$ yields

$$\begin{aligned} E_{\text{inc}}(\xi,\eta) &= E_1 e^{\mathrm{i}(k_{1\xi}\xi + k_\eta \eta)} \\ E_{\text{tr}}(\xi,\eta) &= E_2 e^{\mathrm{i}(k_{2\xi}\xi + k_\eta \eta)} \\ T(\xi,\eta) &= \frac{E_{\text{tr}}}{E_{\text{inc}}} = \frac{E_2}{E_1} e^{\mathrm{i}k_\perp \xi}, \end{aligned} \tag{4.4}$$

where $k_{1\xi} = k_{1x}\cos\theta - k_{1y}\sin\theta$, $k_{2\xi} = k_{2x}\cos\theta - k_{2y}\sin\theta$, and $k_\eta = k_{2x}\sin\theta + k_{2y}\cos\theta$. Most importantly, the hologram grating modulates the phase only along ξ since the phase dependence along η is identical for the incident and transmitted fields. The transmittance has the periodicity $L = 2\pi/k_\perp$ and this is also the local periodicity of the hologram structure.

The electromagnetic field on both sides of the hologram[20] can now be expressed

[19] The compact antenna test range (CATR) holograms have not, however, been designed using this method but rather a parametrised iterative algorithm especially tailored for synthesising plane-wave holograms, see, for instance, in reference [83].

[20] The polarization of the field is ignored in this discussion. Although it plays an important role in the actual implementation of the synthesis algorithms, general principles can be described without explicit reference to the polarization.

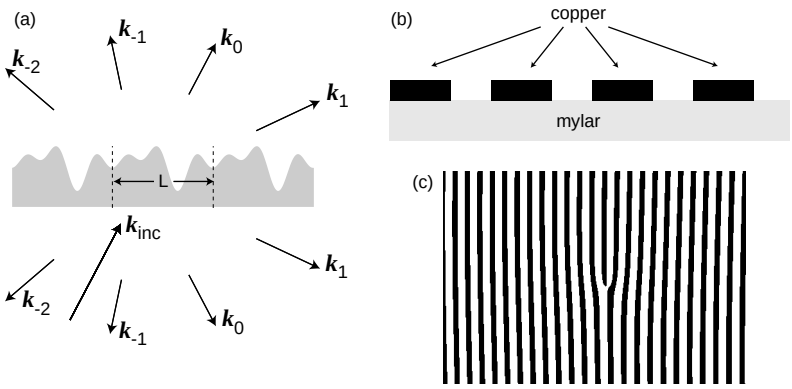

Figure 4.2: (a) Arbitrary periodic grating scatters an incident plane wave into several distinct transmitted and reflected diffraction orders. (b) Grating structure used in radio holograms. Copper stripes layed on a dielectric mylar film essentially reflect all incident waves while the slots in-between allow the radiation be transmitted. (c) Part of a vortex-generating hologram where black denotes copper stripes and white slots.

using the Rayleigh expansions [87]

$$\begin{aligned} E_{z<0} &= E_1 e^{\mathrm{i}(k_{1x}\xi + k_\eta \eta)} + \sum_{n=-\infty}^{\infty} R_n e^{\mathrm{i}(k_{\xi n}\xi + k_\eta \eta - k_{zn} z)} \\ E_{z>0} &= \sum_{n=-\infty}^{\infty} T_n e^{\mathrm{i}(k_{\xi n}\xi + k_\eta \eta + k_{zn} z)}, \end{aligned} \tag{4.5}$$

where $k_{\xi n} = k_{1\xi} + n2\pi/L$ and $k_{zn} = \sqrt{k^2 - k_{\xi n}^2 - k_\eta^2}$. The sums extend over different diffraction orders, either propagating or evanescent, and R_n and T_n are the reflection and transmission coefficients of each order, respectively, see figure 4.2.

Assuming that the field is measured far enough from the hologram such that the diffraction orders have spatially separated as in figure 4.1, only the transmittance T_1 of the first diffraction order contributes to E_{tr}. By construction, it also has exactly the correct phase term since $k_{\xi,n=1} = k_{1\xi} + 2\pi/L = k_{2\xi}$. In order to find the required transmission coefficient T_1, the hologram structure must be modeled, either using a simplified scalar theory or a rigorous theory that models the entire electromagnetic field within the hologram grating, thus taking into account the finite thickness of the structure. Several algorithms for this purpose have been developed within diffractive optics [87].

Choosing the proper structure for a grating period is an inverse problem in the

sense that for a given structure it is possible to find the required coefficient T_1 but, beyond the scalar theory, there are no simple methods to invert the procedure. Hence a limited family of structures is often chosen, such as binary gratings that have one rectangular groove of a variable thickness and width per period. The transmission may then be calculated for different values of the parameters and the optimal choice be taken. In particular, the phase of the transmission T_1 can always be matched to coincide with the phase of the field required, E_{tr}, with the use of a translation of the grating structure [88]. Each family of structures still has a maximum transmission amplitude that can not be exceeded. Within these constraints, a binary grating can be used to produce an arbitrary transmittance. The more degrees of freedom is allowed for the family of different structures, the more energy can usually be directed into the first diffraction order; in this sense the binary grating is still limited in applicability.

4.2 Experimental results

Several different types of holograms have been produced and measured in order to test and verify the synthesis methods employed and to experimentally study the propagation of apertured electromagnetic beams. A radio source of the frequency 310 GHz (wavelength $\lambda = 0.97$ mm) and of linear polarization was used and all measurements in this section were obtained using scalar-theory amplitude holograms. The measurement setup and details (together with some further experiments not mentioned here) are described in [VIII].

4.2.1 Plane-wave vortex

Electromagnetic vortices are radio-wave fields that contain phase singularities where the field amplitude necessarily vanishes [36]. The trajectory of the singularity in the centre of a circular radio-wave field is a straight line[21] and it can thus be used to align the electromagnetic beam.

A hologram was synthesised to produce the radio field

$$E(r', \varphi') = W(r')e^{\mathrm{i}\varphi'}, \tag{4.6}$$

where r' is the radial coordinate and φ' is the azimuthal angle in the beam coordinates. The exponential term produces the phase singularity at $r' = 0$ while the amplitude $W(r')$ is a constant disc of radius 10 cm, tapered on the boundary to reduce edge diffraction. Although the amplitude is not explicitly required to vanish at $r' = 0$, it is necessarily bound to do so during the actual beam propagation.

[21] For more complex situations, see, e.g., reference [89].

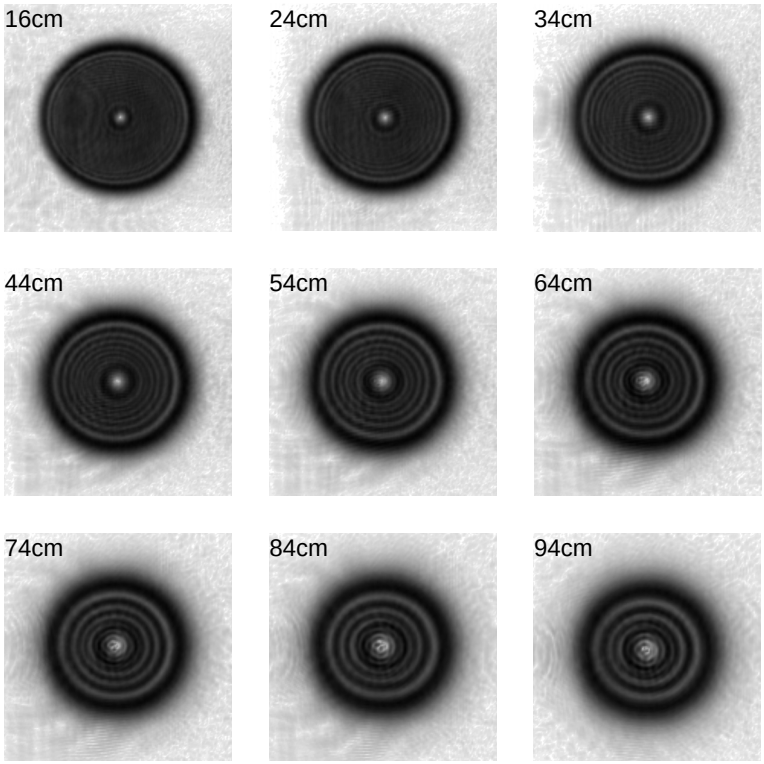

Figure 4.3: Propagation of an electromagnetic vortex. The vortex core remains unchanged while the rest of the apertured field develops diffraction rings. Area illustrated in each figure is 6 cm $\times$ 6 cm and the gray scale is linear in field amplitude.

The beam was measured at several distances from 16 cm to 94 cm in order to study the propagation of the vortex, see figure 4.3. The vortex core itself is seen to remain unchanged until the approximate distance of 70 cm, after which ripples start to develop in the vicinity of the core. The phase singularity, however, remains in the core and the amplitude vanishes at the singularity. The rest of the disc is subject to edge diffractions and increasing diffraction rings are observed. Comparison with simulations attribute the rings to the aperture radius and to the particular tapering used.

4.2.2 Bessel beam

Propagation of the Bessel beam was investigated with the use of a zeroth-order Bessel-beam hologram. The hologram was designed to produce only the inward-propagating component of the beam in order to yield a diamond-shaped area of the Bessel beam,

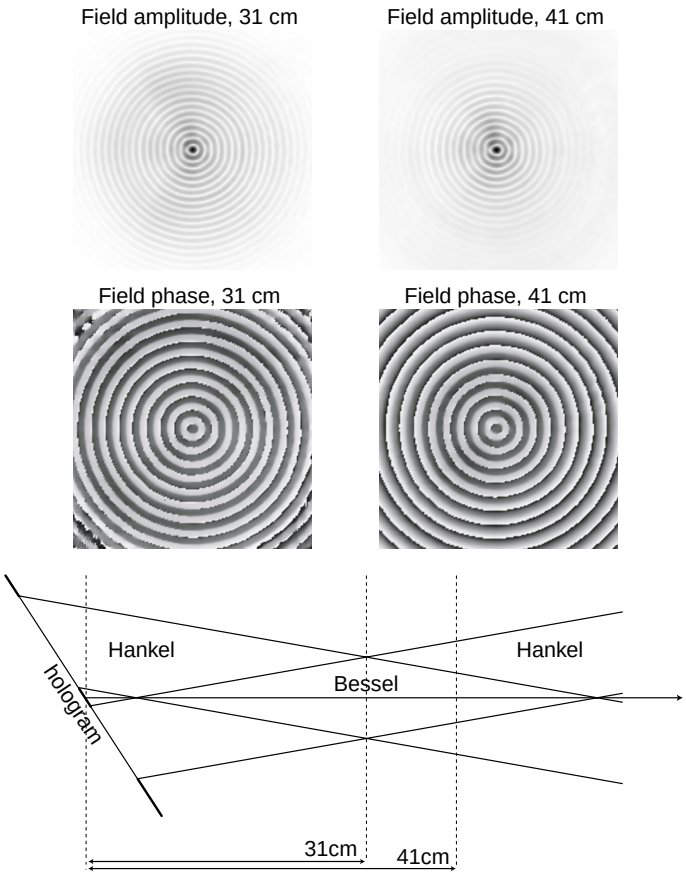

Figure 4.4: Apertured Bessel beam. Areas illustrated are 9.6 cm × 9.6 cm.

see figure 4.4. The hologram was tapered both in the center and on the outer aperture boundary; the central tapering increases the total efficiency since, otherwise, the highest amplitude would be produced there and the transmittance in the outer regions should be reduced accordingly.

The beam measured at the waist shows a clear Bessel-beam structure that vanishes approximately at the geometric boundary caused by the aperture. The phase is binary, reflecting the fact that the beam is, in fact, created as a standing-wave pattern of the inward and of the outward propagating components. The phase ripples near the corners are due to the nearly vanishing field whose phase varies stochastically in the measurement. The field following the geometric waist retains its Bessel-beam character at the centre but, in the outer regions, it transforms into a Hankel-type wave. This is observed both in the amplitude and in the phase: the superposition pattern vanishes and it is transformed into a decreasing $r^{-1/2}$ amplitude while the binary phase is

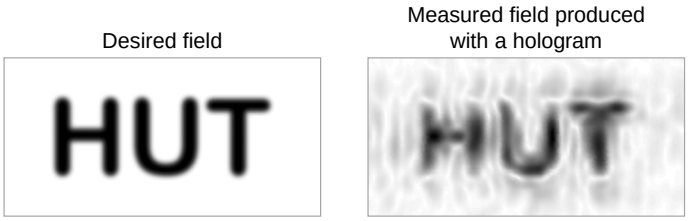

Figure 4.5: Field produced with a back-propagation designed hologram. Area illustrated is 16 cm × 8 cm. This measurement has been published in [90].

simultaneously changed into a linearly increasing phase.

4.2.3 Custom-made wave field

We produced a custom-made hologram in order to verify the applicability of the back-propagation scheme for radio holograms. The desired radio field was composed of the letters 'HUT' (standing for Helsinki University of Technology) and the hologram was designed to form this field pattern at the distance of 1 m from the hologram. The desired field together with the final measurement are shown in figure 4.5.

The text HUT is clearly identified in the measured field, despite the external field noise. The transmittance obtained with the use of the back propagation was highly complicated and the measured field proves the usefulness of the back-propagation design method. Rigorous optimisation of the hologram structure should yield yet an improved contrast to the field produced.

5 Summary

The physical phenomena considered in this thesis are, in principle, electromagnetic and acoustic wave propagation in homogeneous, linear, and nondispersive media, in particular in free space and in anisotropic crystals. The phenomenology of waves is, however, rich and it gives rise to wave forms of very specific properties, such as both axial and radial localisation or propagation invariance.

In this thesis, the concept of rotationally periodic waves is introduced and applied as a framework for the analysis of waves that remain localised under propagation in free space; both the nondiffracting waves and the focus-wave modes belong to this class of waves. Rotationally periodic waves can also be understood as pulsed variants of self-imaging fields that have been widely studied using diffractive optics. The key feature underlying their properties is the synchronous generation of conical waves that approach the optical axis so as to continually reconstruct the exact pulse profile. Physically, no propagation invariance may occur endlessly since the waves should eventually be launched arbitrarily far from the axis, requiring an infinite-size apparatus; practically, these waves can still be formed for a long-enough propagation distances to allow their use in experiments and applications.

Two more specialised issues are also considered in this thesis: (i) The theoretical treatment of nondiffracting waves is extended to anisotropic media where the phenomena inherent to strong anisotropy are also portrayed in the nondiffracting waves. (ii) Radio holograms have been used to experimentally verify the propagation of Bessel beams, as well as of other types of radio beams. These two specific cases are to exemplify different fields of physics where propagation-invariant waves are producible and appliable.

References

[1] J. Durnin, J. J. Miceli, Jr., and J. H. Eberly, *Diffraction-free beams*, Phys. Rev. Lett. **58**, pp. 1499–1501 (1987).

[2] F. Gori, G. Guattari, and C. Padovani, *Bessel-Gauss beams*, Opt. Commun. **64**, pp. 491–495 (1987).

[3] J. A. Stratton, *Electromagnetic Theory*, pp. 354–357 (McGraw-Hill, New York and London, 1941).

[4] A. G. van Nie, *Rigorous calculation of the electromagnetic field of wave beams*, Philips Res. Reports **19**, pp. 378–394 (1964).

[5] J. J. O'Connor and E. F. Robertson, *Friedrich wilhelm bessel*, http://www-gap.dcs.st-and.ac.uk/∼history/Mathematicians/Bessel.html (1997).

[6] J. H. McLeod, *The axicon: a new type of optical element*, J. Opt. Soc. Am. A **44**, pp. 591–597 (1954).

[7] J. H. McLeod, *Axicons and their uses*, J. Opt. Soc. Am. A **50**, pp. 166–169 (1960).

[8] D. H. Kelly, *Axicons, annuli, and coherent light*, J. Opt. Soc. Am. **53**, p. 525 (1963).

[9] F. V. Bunkin, V. V. Korobkin, Y. A. Kurinyi, L. Y. Polonskii, and L. N. Pyatnitskii, *Laser spark with a continuous channel in air*, Sov. J. Quantum Electron. **13**, pp. 254–255 (1983).

[10] V. V. Korobkin, L. Y. Polonskii, V. P. Poponin, and L. N. Pyatnitskii, *Focusing of Gaussian and super-Gaussian laser beams by axicons to obtain continuous laser sparks*, Sov. J. Quantum Electron. **16**, pp. 178–182 (1986).

[11] C. W. McCutchen, *Generalized aperture and three-dimensional diffraction image*, J. Opt. Soc. Am. **54**, pp. 240–244 (1964).

[12] G. Indebetouw, *Nondiffracting optical fields: Some remarks on their analysis and synthesis*, J. Opt. Soc. Am. A **6**, pp. 150–152 (1989).

[13] G. Scott and N. McArdle, *Efficient generation of nearly diffraction-free beams using an axicon*, Opt. Engineer. **31**, pp. 2640–2643 (1992).

[14] D. K. Hsu, F. J. Margetan, and D. O. Thompson, *Bessel beam ultrasonic transducer: Fabrication method and experimental result*, Appl. Phys. Lett. **55**, pp. 2066–2068 (1989).

[15] J.-y. Lu and J. F. Greenleaf, *Ultrasonic nondiffracting transducer for medical imaging*, IEEE Trans. Ultrason., Ferroelec., Freq. Contr. **37**, pp. 438–447 (1990).

[16] J.-y. Lu and J. F. Greenleaf, *Nondiffracting X waves — Exact solutions to free-space scalar wave equation and their finite aperture realizations*, IEEE Trans. Ultrason., Ferroelec., Freq. Contr. **39**, pp. 19–31 (1992).

[17] J. Fagerholm, A. T. Friberg, J. Huttunen, D. P. Morgan, and M. M. Salomaa, *Angular-spectrum representation of nondiffracting X waves*, Phys. Rev. E **54**, pp. 4347–4352 (1996).

[18] P. Saari and K. Reivelt, *Evidence of X-shaped propagation-invariant localized light waves*, Phys. Rev. Lett. **79**, pp. 4135–4138 (1997).

[19] J. Durnin, *Exact solutions for nondiffracting beams. I. The scalar theory*, J. Opt. Soc. Am. A **4**, pp. 651–654 (1987).

[20] J. N. Brittingham, *Focus wave modes in homogeneous Maxwell's equations: Transverse electric mode*, J. Appl. Phys. **54**, pp. 1179–1189 (1983).

[21] A. Sezginer, *A general formulation of focus wave modes*, J. Appl. Phys. **57**, pp. 678–683 (1985).

[22] A. M. Shaarawi, *Comparison of two localized wave fields generated from dynamic apertures*, J. Opt. Soc. Am. **14**, pp. 1804–1816 (1997).

[23] J.-y. Lu, *Experimental study of high frame rate imaging with limited diffraction beams*, IEEE Trans. Ultrason., Ferroelec., Freq. Contr. **45**, pp. 84–97 (1998).

[24] M. Erdélyi, Z. L. Horváth, G. Szabó, Z. Bor, F. K. Tittel, J. R. Cavallaro, and M. C. Smayling, *Generation of diffraction-free beams for applications in optical microlithography*, J. Vac. Science & Techn. B **15**, pp. 287–292 (1997).

[25] K. M. Iftekharuddin and M. A. Karim, *Heterodyne detection by using a diffraction-free beam: tilt and offset effects*, Appl. Opt. **31**, pp. 4853–4856 (1992).

[26] M. Nisoli, E. Priori, G. Sansone, S. Stagira, G. Cerullo, and S. D. Silvestri, *High-brightness high-order harmonic generation by truncated Bessel beams in the sub-10-fs regime*, Phys. Rev. Lett. **88**, p. 033902 (2002).

[27] T. Wulle and S. Herminghaus, *Nonlinear optics of Bessel beams*, Phys. Rev. Lett. **70**, pp. 1401–1404 (1993).

[28] B. Glushko, B. Kryzhanovsky, and D. Sarkisyan, *Self-phase-matching mechanism for efficient harmonic generation processes in a ring pump beam geometry*, Phys. Rev. Lett. **71**, pp. 243–246 (1993).

[29] V. Garcés-Chávez, D. McGloin, H. Melville, W. Sibbett, and K. Dholakia, *Simultaneous micromanipulation in multiple planes using a self-reconstructing light beam*, Nature **419**, pp. 145–147 (2002).

[30] A. T. Friberg, J. Fagerholm, and M. M. Salomaa, *Space-frequency analysis of nondiffracting pulses*, Opt. Commun. **136**, pp. 207–212 (1997).

[31] S. Chávez-Cerda, *A new approach to Bessel beams*, J. Mod. Opt. **46**, pp. 923–930 (1999).

[32] J. Durnin and J. J. Miceli, Jr., *Comparison of Bessel and Gaussian beams*, Opt. Lett. **13**, pp. 79–80 (1988).

[33] P. Sprangle and B. Hafizi, *Comment on nondiffracting beams*, Phys. Rev. Lett. **66**, p. 837 (1991).

[34] J. Durnin, J. J. Miceli, Jr., and J. H. Eberly, *Reply on 'comment on nondiffracting beams'*, Phys. Rev. Lett. **66**, p. 838 (1991).

[35] S. Chávez-Cerda, G. S. McDonald, and G. H. C. New, *Nondiffracting beams: Travelling, standing, rotating and spiral waves*, Opt. Commun. **123**, pp. 225–233 (1996).

[36] G. Indebetouw, *Optical vortices and their propagation*, J. Mod. Opt. **40**, pp. 73–87 (1993).

[37] K. Volke-Sepulveda, V. Garcés-Chávez, S. Chávez-Cerda, J. Arlt, and K. Dholakia, *Orbital angular momentum of a high-order Bessel light beam*, J. Opt. B **4**, pp. S82–S89 (2002).

[38] R. Piestun and J. Shamir, *Generalized propagation-invariant wave fields*, J. Opt. Soc. Am. A **15**, pp. 3039–3044 (1998).

[39] R. Donnelly, D. Power, G. Templemen, and A. Whalen, *Graphical simulation of superluminal acoustic localized wave pulses*, IEEE Trans. Ultrason., Ferroelec., Freq. Contr. **41**, pp. 7–12 (1994).

[40] J. W. Goodman, *Introduction to Fourier optics*, 2 ed. (McGraw-Hill, New-York, 1996).

[41] E. Heyman, *Focus wave modes: a dilemma with causality*, IEEE Trans. Antennas Propagat. **37**, pp. 1604–1608 (1989).

[42] E. Recami, *On localized 'X-shaped' superluminal solutions to Maxwell equations*, Physica A **252**, pp. 586–601 (1998).

[43] S. R. Mishra, *A vector wave analysis of a Bessel beam*, Opt. Commun. **85**, pp. 159–161 (1991).

[44] Z. Bouchal, R. Horak, and J. Wagner, *Propagation-invariant electromagnetic fields: theory and experiment*, J. Mod. Opt. **43**, pp. 1905–1920 (1996).

[45] Z. Bouchal and M. Olivík, *Non-diffractive vector Bessel beams*, J. Mod. Opt. **42**, pp. 1555–1566 (1995).

[46] T. T. Wu and R. W. P. King, *Comment on 'focus wave modes in homogeneous Maxwell's equations: Transverse electric mode'*, J. Appl. Phys. **56**, pp. 2587–2588 (1984).

[47] R. W. Ziolkowski and D. K. Lewis, *Evidence of localized wave transmission*, Phys. Rev. Lett. **62**, pp. 147–1989 (1989).

[48] A. M. Shaarawi, I. M. Besieris, R. W. Ziolkowski, and S. M. Sedky, *Generation of approximate focus-wave-mode pulses from wide-band dynamic Gaussian apertures*, J. Opt. Soc. Am. **12**, pp. 1954–1964 (1995).

[49] P. T. M. Hillion, *Nondispersive waves: Interpretation and causality*, IEEE Trans. Antennas Propagat. **40**, pp. 1031–1035 (1992).

[50] E. Heyman and L. B. Felsen, *Comment on "nondispersive waves: Interpretation and causality"*, IEEE Trans. Antennas Propagat. **42**, pp. 1668–1670 (1994).

[51] A. M. Shaarawi, R. W. Ziolkowski, and I. M. Besieris, *On the evanescent fields and the causality of the focus wave modes*, J. Math. Phys **36**, pp. 5565–5587 (1995).

[52] P. Saari and H. Sõnajalg, *Pulsed Bessel beams*, Laser Phys. **7**, pp. 32–39 (1997).

[53] W. Hu and H. Guo, *Ultrashort pulsed Bessel beams and spatially induced group-velocity dispersion*, J. Opt. Soc. Am. A **19**, pp. 49–53 (2002).

[54] J. Turunen, A. Vasara, and A. T. Friberg, *Holographic generation of diffraction-free beams*, Appl. Opt. **27**, pp. 3959–3962 (1988).

[55] A. Vasara, J. Turunen, and A. T. Friberg, *Realization of general nondiffracting beams with computer-generated holograms*, J. Opt. Soc. Am. A **6**, pp. 1748–1754 (1989).

[56] J.-y. Lu and J. F. Greenleaf, *Pulse-echo imaging using a nondiffracting beam transducer*, Ultras. Med. Biol. **17**, pp. 265–281 (1991).

[57] R. W. Ziolkowski, *Localized transmission of electromagnetic energy*, Phys. Rev. A **39**, pp. 2005–2033 (1989).

[58] K. M. Iftekharuddin, A. A. S. Awwal, and M. A. Karim, *Gaussian-to-Bessel beam transformation using a split refracting system*, Appl. Opt. **32**, pp. 2252–2256 (1993).

[59] M. Arif, M. M. Hossain, A. A. S. Awwal, and M. N. Islam, *Refracting system for annular Gaussian-to-Bessel beam transformation*, Appl. Opt. **37**, pp. 649–652 (1998).

[60] P. L. Overfelt, *Bessel-Gauss pulses*, Phys. Rev. A **44**, pp. 3941–3947 (1991).

[61] P. L. Overfelt and C. S. Kenney, *Comparison of the propagation characteristics of Bessel, Bessel-Gauss, and Gaussian beams diffracted by a circular aperture*, J. Opt. Soc. Am. A **8**, pp. 732–745 (1991).

[62] R. Piestun, Y. Y. Schechner, and J. Shamir, *Propagation-invariant wave fields with finite energy*, J. Opt. Soc. Am. A **17**, pp. 294–303 (2000).

[63] R. Weigel, D. P. Morgan, J. M. Owens, A. Ballato, K. M. Lakin, K.-y. Hashimoto, and C. C. W. Ruppel, *Microwave acoustic materials, devices, and applications*, IEEE Trans. Microwave Theory Tech. **50**, pp. 738–749 (2002).

[64] J. P. Wolfe, *Imaging phonons: acoustic wave propagation in solids* (Cambridge University Press, Cambridge, 1998).

[65] J. V. Knuuttila, P. T. Tikka, and M. M. Salomaa, *Scanning Michelson interferometer for imaging surface acoustic wave fields*, Opt. Lett. **25**, pp. 613–615 (2000).

[66] Y. Sugawara, O. B. Wright, O. Matsuda, M. Takigahira, Y. Tanaka, S. Tamura, and V. E. Gusev, *Watching ripples on crystals*, Phys. Rev. Lett. **88**, p. 185504 (2002).

[67] B. Taylor, H. J. Maris, and C. Elbaum, *Phonon focusing in solids*, Phys. Rev. Lett. **23**, pp. 416–419 (1969).

[68] B. Taylor, H. J. Maris, and C. Elbaum, *Focusing of phonons in crystalline solids due to elastic anisotropy*, Phys. Rev. B **3**, pp. 1462–1472 (1971).

[69] M. Born and E. Wolf, *Principles of Optics*, 6 ed. (Pergamon Press, Oxford, 1997).

[70] L. D. Landau and E. M. Lifshitz, *Theory of Elasticity*, 3 ed. (Pergamon Press, London, 1986).

[71] M. A. Auld, *Acoustic fields and waves in solids*, vol. 1 (John Wiley & Sons, New York, 1973).

[72] N. W. Ashcroft and N. D. Mermin, *Solid State Physics* (Saunders, Philadelphia, 1976).

[73] J. H. Staudte and B. D. Cook, *Visualization of quasilongitudinal and quasitransverse elastic waves*, J. Acoust. Soc. Am. **41**, pp. 1547–1548 (1967).

[74] H. J. Maris, *Effect of finite phonon wavelength on phonon focusing*, Phys. Rev. B **28**, pp. 7033–7037 (1983).

[75] J.-y. Lu, X. Xu, and J. F. Greenleaf, *A new approach to obtain limited diffraction beams*, IEEE Trans. Ultrason., Ferroelec., Freq. Contr. **42**, pp. 850–853 (1995).

[76] M. F. Lewis, *High frequency acoustic plate mode employing interdigital transducer*, Electron. Lett. **17**, pp. 819–821 (1981).

[77] M. A. Goodberlet and D. L. Lee, *The excitation and detection of surface-generated bulk waves*, IEEE Trans. Ultrason., Ferroelec., Freq. Contr. **SU-31**, pp. 67–76 (1984).

[78] D. P. Morgan, *Surface-wave devices for signal processing* (Elsevier, Amsterdam, 1985).

[79] C. K. Campbell, *Surface Acoustic Wave Devices for Mobile and Wireless Communications* (Academic Press, London, 1998).

[80] J. V. Knuuttila, J. Saarinen, C. S. Hartmann, V. P. Plessky, and M. M. Salomaa, *Measurement of BAW radiation from low-loss LSAW resonators*, Electron. Lett. **37**, pp. 1055–1056 (2001).

[81] D. Gabor, *A new microscope principle*, Nature **161**, pp. 777–778 (1948).

[82] W.-H. Lee, *Computer-generated holograms: Techniques and applications*, in *Progress in Optics XVI*, edited by E. Wolf, pp. 121–231 (Elsevier, Amsterdam, 1978).

[83] T. Hirvonen, J. P. S. Ala-Laurinaho, J. Tuovinen, and A. V. Räisänen, *A compact antenna test range based on a hologram*, IEEE Trans. Antennas Propagat. **45**, pp. 1270–1276 (1997).

[84] J. Ala-Laurinaho, T. Hirvonen, P. Piironen, A. Lehto, J. Tuovinen, A. V. Räisänen, and U. Frisk, *Measurement of the Odin telescope at 119 GHz with a hologram-type CATR*, IEEE Trans. Antennas Propagat. **49**, pp. 1264–1270 (2001).

[85] S. Monk, J. Arlt, D. A. Robertson, J. Courtial, and M. J. Padgett, *The generation of Bessel beams at millimetre-wave frequencies by use of an axicon*, Opt. Commun. **170**, pp. 213–215 (1999).

[86] J. Tervo and J. Turunen, *Generation of vectorial propagation-invariant fields by polarization-grating axicons*, Opt. Commun. **192**, pp. 13–18 (2001).

[87] R. Petit, editor, *Electromagnetic theory of gratings* (Springer-Verlag, Berlin, 1980).

[88] A. W. Lohmann and D. P. Paris, *Binary Fraunhofer holograms, generated by computer*, Appl. Opt. **6**, pp. 1739–1748 (1967).

[89] I. Freund, *Optical vortex trajectories*, Opt. Commun. **181**, pp. 19–33 (2000).

[90] J. Meltaus, J. Salo, E. Noponen, M. M. Salomaa, V. Viikari, A. Lönnqvist, T. Koskinen, J. Säily, J. Häkli, J. Ala-Laurinaho, J. Mallat, and A. V. Räisänen, *Radio-wave beam shaping using holograms*, in *IEEE MTT-S International Microwave Symposium Digest*, pp. 1305–1308 (IEEE, New York, 2002).

Abstracts of publications I–VIII

I We consider periodically propagating pulses, devoid of diffractive spreading. They may feature arbitrary velocities of propagation but their spectral characteristics vary according to whether they are luminal, subluminal or superluminal. The wave modes introduced are closely related to the X waves and the focus wave modes, but they allow a frequency-dependent cone angle and they are not limited to the speed of light.

II We introduce subsonic nondiffracting waves which — unlike the ordinary supersonic nondiffracting waves — evolve periodically under propagation. Such pulse-like waves have a subsonic uniformly propagating 'core', which is modulated by a supersonic plane wave. The subsonic core may also be considered an envelope for a truncated Bessel beam and subsonic nondiffracting waves may be used to describe signal propagation within Bessel beams.

III A unified spectral and temporal representation is introduced for nondiffracting waves. We consider a set of elementary broadband X waves which spans the commonly considered nondiffracting wave solutions. These basis X waves have a simple spectral representation which leads to expressions in closed algebraic form or, alternatively, in terms of hypergeometric functions. The span of the X waves is also closed with respect to all spatial and temporal derivatives and, consequently, they can be used to compose different types of waves with complex spectral and spatial properties. The unified description of Bessel-based nondiffracting waves is further extended to include singular Neumann and Hankel waves, or Y waves. We also discuss connections between the different known nondiffracting wave solutions, and their relations to the present unified approach.

IV Nondiffracting pulses are spatially and temporally localized wave fields that undergo no diffractive spreading under propagation through homogeneous media. We introduce an orthogonality condition for nondiffracting pulses and present an orthogonal set of X waves which possess temporal spectra of the form (polynomial in ω)$\times e^{-\alpha\omega}$. The newly introduced Bessel-X pulses and X-wave transforms are discussed in the framework of orthogonal X-wave bases.

V The concept of nondiffracting waves is generalized to encompass bulk-acoustic waves within crystalline media. We introduce acoustic Bessel beams and generalized X waves for anisotropic elastic materials. Detailed numerical predictions for propagation-invariant bulk-acoustic beams of various orders, and also X pulses, are presented for experimental verification. The materials parameters used have been chosen appropriate for quartz, the most important material for acoustic device applications.

VI Recently, the physics of ballistic phonon propagation in anisotropic crystals has been studied with new phonon-imaging methods. In this paper we consider nondiffracting waves that can propagate in anisotropic crystals and analyze their properties that emerge specifically due to the anisotropy. We further present a detailed generation and detection scheme for the experimental verification of the wave modes considered.

VII A computer-generated binary amplitude hologram is used to transform an initial Gaussian electromagnetic field with spherical phase front at 310 GHz into a nondiffracting Bessel beam. The beam profile is measured with the help of a near-field scanner. In contrast to the situation in the optical region, both amplitude and phase information is readily obtainable from the generated field.

VIII Holograms — diffractive elements — are designed and fabricated for shaping millimetre-wave radio fields. Methods for the synthesis of hologram elements are discussed and several beam shapes are tested: plane waves, radio-wave vortices, and Bessel beams. Here we present an overview of the methods applied and results obtained with quasi-optical hologram techniques using both amplitude and phase holograms.

ISBN 951-22-6292-4
ISSN 1456-3320